NASA SP-8017

NASA
SPACE VEHICLE
DESIGN CRITERIA
[ENVIRONMENT]

MAGNETIC FIELDS — EARTH AND EXTRATERRESTRIAL

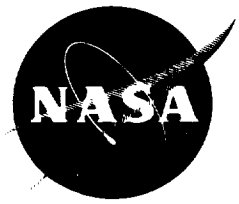

MARCH 1969

NATIONAL AERONAUTICS AND SPACE ADMINISTRATION

FOREWORD

NASA experience has indicated a need for uniform design criteria for space vehicles. Accordingly, criteria are being developed in the following areas of technology:

Environment
Structures
Guidance and Control
Chemical Propulsion

Individual components will be issued as separate monographs as soon as they are completed. A list of all previously issued monographs in this series can be found on the last page of this publication.

These monographs are to be regarded as guides to design and not as NASA requirements, except as may be specified in formal project specifications. It is expected, however, that the criteria sections of these documents, revised as experience may indicate to be desirable, eventually will become uniform design requirements for NASA space vehicles.

This monograph was prepared under the cognizance of the Goddard Space Flight Center (GSFC) with Scott A. Mills and John J. Sweeney as program coordinators. Mark Harris and Robert Lyle of Exotech Incorporated, Washington, D.C., were the principal authors. Major contributions were made by Earl Clifford of Exotech and Robert Fischell of the Applied Physics Laboratory, Johns Hopkins University. An Advisory Panel provided guidance in determining the monograph's scope and assuring its technical validity. The following individuals served as members:

Mr. Andrew J. Beck	Jet Propulsion Laboratory California Institute of Technology
Mr. Joseph C. Boyle	Goddard Space Flight Center
Mr. William G. Brown	Goddard Space Flight Center
Dr. Laurence J. Cahill	Univ. of Minnesota
Mr. P. Chinberg	Univ. of New Hampshire
Dr. Paul J. Coleman	Univ. of California, Los Angeles
Mr. Harold C. Euler	Marshall Space Flight Center
Mr. Robert E. Fischell	Applied Physics Laboratory Johns Hopkins University
Dr. R. T. Frost	General Electric Company
Mr. Robert E. Gebhardt	Goddard Space Flight Center
Mr. Lynn Grasshoff	Hughes Aircraft Company
Dr. Ernest J. Iufer	Ames Research Center
Mr. Ernest J. Mosher	Goddard Space Flight Center

Mr. C. Leland Parsons	Goddard Space Flight Center
Mr. Clell S. Scearce	Goddard Space Flight Center
Mr. Robert Snare	Univ. of California, Los Angeles

Comments concerning the technical content of these monographs will be welcomed by the National Aeronautics and Space Administration, Office of Advanced Research and Technology (Code RVA), Washington, D.C. 20546.

March 1969

For sale by the Clearinghouse for Federal Scientific and Technical Information
Springfield, Virginia 22151 – Price $3.00

CONTENTS

MAGNETIC FIELDS— EARTH AND EXTRATERRESTRIAL

1. INTRODUCTION

Natural magnetic fields as well as induced fields are important considerations in space vehicle design because they can adversely affect onboard equipment and scientific instrumentation and can change an orbiting spacecraft's drag, attitude, and direction of motion. For example, the magnetic torques resulting from the interaction between the ambient magnetic field and the spacecraft's magnetic properties may degrade the performance of the attitude control system (ref. 1).

This monograph presents the information on the strength and direction of the natural magnetic fields needed for vehicle design. These fields include the geomagnetic field (confined to the volume of space about Earth called the magnetosphere), the interplanetary field (Sun's field), and the fields of the planets and their natural satellites. Knowledge of these natural magnetic fields is increasing rapidly, but the present state of knowledge limits the availability of a definitive analytical model of the Earth's main (geomagnetic) field to about 6.6 Earth radii (synchronous altitude) as presented herein. For the regions beyond this altitude, the available information has been reviewed to determine both quantitative and qualitative data useful for design purposes.

Induced magnetic fields encountered during manufacture, testing, and transportation of spacecraft can cause undesirable magnetic properties to be introduced into spacecraft. These fields warrant careful consideration and control in order to achieve "magnetic cleanliness" of spacecraft—the subject of a separate monograph. References 2 and 3 provide some information on this subject.

2. STATE OF THE ART

Extensive observations of the magnetic field on and above the Earth's surface have been made for more than a century. Recent data from space exploration have changed the concept of the geomagnetic field from one of a simple dipolar field to that of the magnetosphere illustrated in figure 1 (ref. 4). This figure shows that the solar plasma flow (solar wind) compresses the Earth's main field on the subsolar side and extends it as a long tail (magnetotail) in the antisolar region. The interaction of the solar wind with the Earth's main field creates a shock front on the subsolar side. Between this shock front and a boundary layer (magnetopause) is a region of solar wind and interplanetary field turbulence called the magnetosheath. The interplanetary field is deflected around Earth's main field at the magnetopause which delineates the extent of the Earth's main field into space.

Figure 2 (ref. 5) illustrates a useful concept of the solar wind interaction with Earth's main field advanced by V.C.A. Ferraro and S. Chapman in 1931. The solar wind, which is an

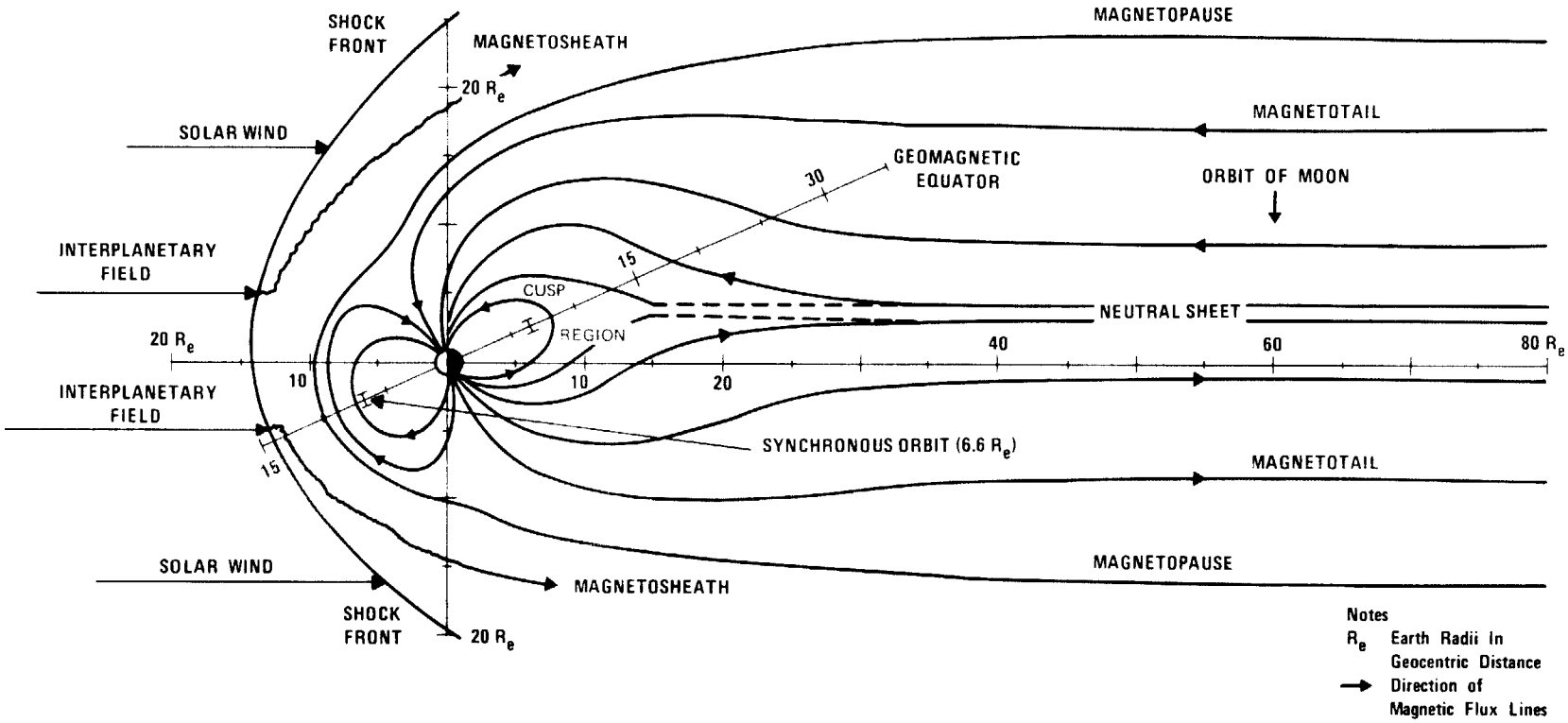

Figure 1.—The magnetosphere (ref. 4).

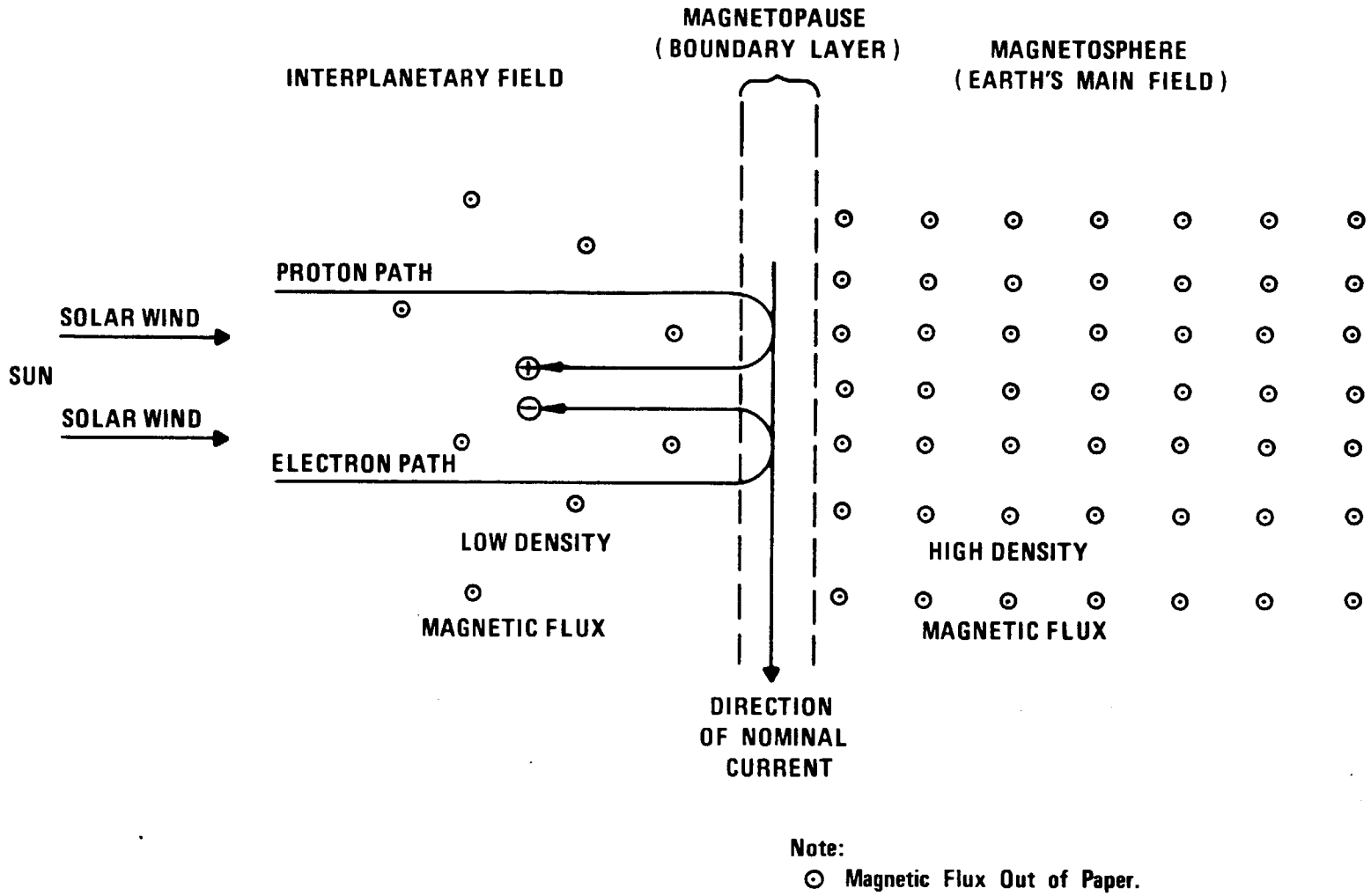

Figure 2.–Ferraro-Chapman model of magnetospheric compression (ref. 5).

electrically neutral plasma consisting mostly of protons and electrons, impinges on the magnetopause. The interaction of these charged particles with the Earth's main field causes the particles to be deflected away from the magnetosphere, an action which generates a current at the magnetopause. The deflected particles are swept around the magnetosphere by the solar wind.

2.1 Earth's Main Field

The Earth's main field is an internally generated magnetic field that resembles the magnetic field of a dipole and extends throughout the magnetosphere. The axis of the dipole passes through northern Greenland at 78.5° N and 69.0° W and has an inclination of about 11.5° with the Earth's axis of rotation (ref. 6).

2.1.1 Surface Geomagnetic Field

The surface geomagnetic field consists of the main field generated within the Earth and all external field components that are measurable at the Earth's surface. The surface intensity ranges from about 0.3 gauss (3×10^{-5} T)* at the equator to about 0.7 gauss (7×10^{-5} T) at the poles as illustrated in figure 3 (ref. 7). Departures of the field from a dipole field are called anomalies. These anomalies are both regional and local. Regional anomalies, such as the South Atlantic anomally, cause irregularities in the surface field over an area of several thousand square kilometers. Local anomalies cause irregularities of about .01 gauss (10^3 nT) or less over an area of a few square kilometers to several hundred square kilometers.

Measurements of the geomagnetic field intensity and direction have been made by observatories, magnetic survey ships, and more recently by instrumented aircraft in data collection efforts. The most recent charts of geomagnetic field data at the Earth's surface for various geographical regions are listed in "Catalog of Nautical Charts and Publications, 1968" (ref. 8) and are available from the U. S. Naval Oceanographic Office**. Magnetic measurements are referenced to geographical or geomagnetic dipole coordinate systems. Figure 4 (ref. 9) illustrates the relationship of coordinate systems for the Earth's surface which are based on the average dipole axis (geomagnetic dipole coordinates) and the spin axis (geographic or geodetic coordinates).***

Magnetic measurements indicate the existence of secular and temporal variations in the surface geomagnetic field.

* Dimensions, units, and conversion factors are defined in appendix B.

** U.S. Naval Oceanographic Office, Suitland, Maryland 20390. Hydrographic Surveys Department, Magnetics Division.

*** Appendix A presents a summary of the coordinate systems commonly used in magnetic field studies and mentioned in this monograph.

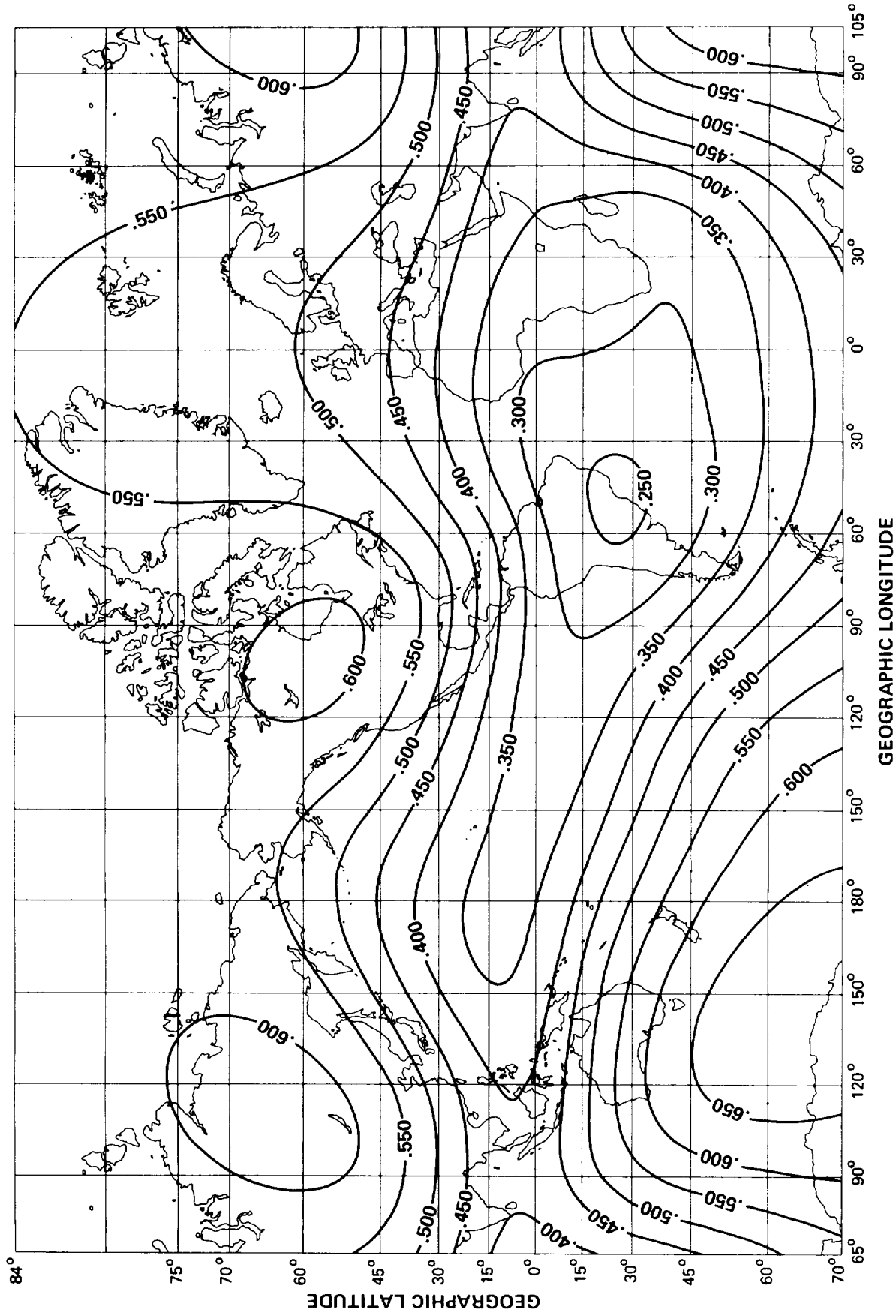

Figure 3.–Total magnetic field intensity at Earth's surface in Gauss (Epoch 1965) (ref. 7).

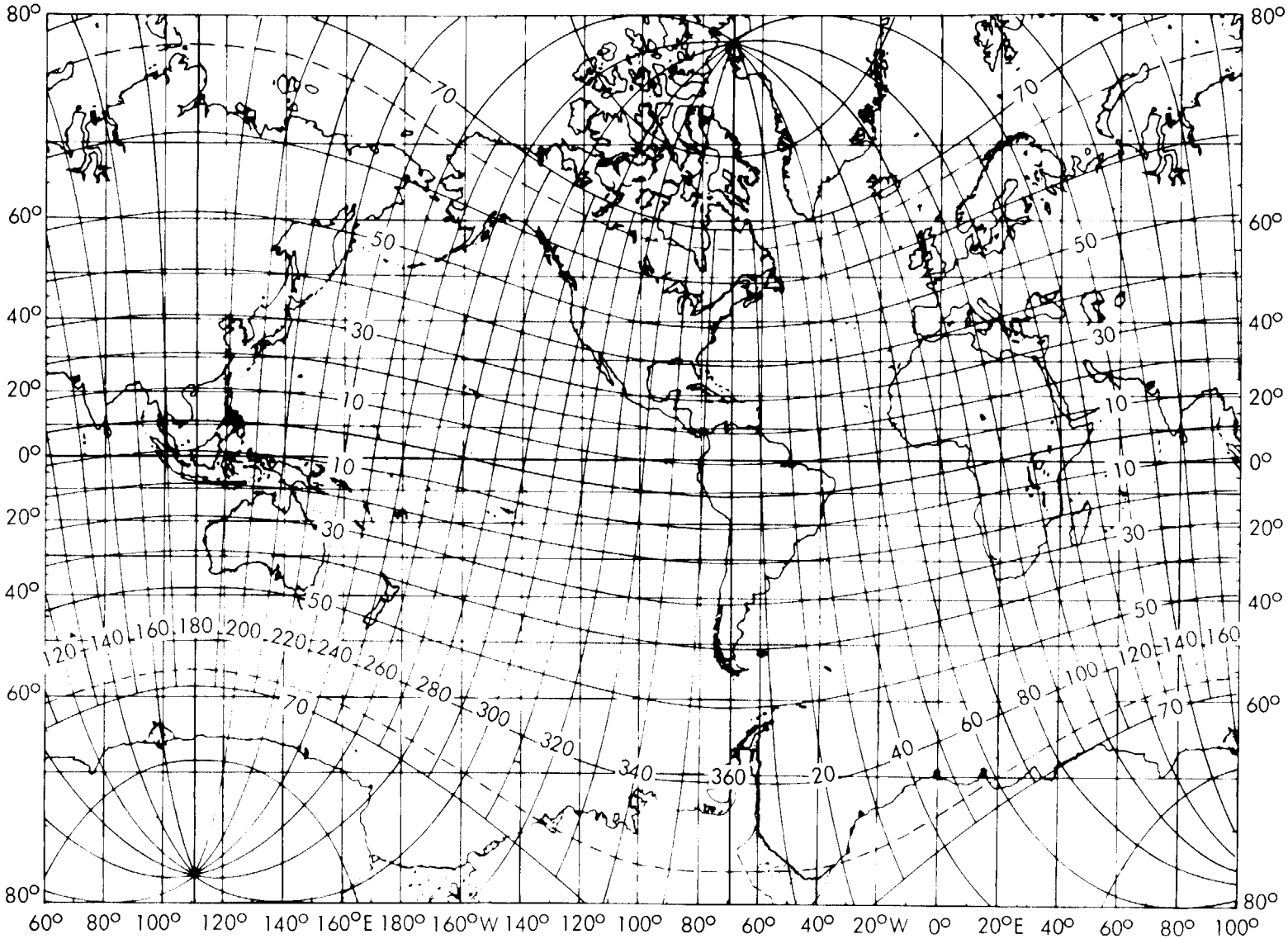

Figure 4.–Comparison of geographical and geomagnetic dipole coordinate system (ref. 9).

The curved lines are the geomagnetic dipole coordinates superposed on a geographic Mercator projection.

2.1.2 Secular Variations

Secular variations are long-term, small magnitude field changes that are measured in terms of years. The predictability of these variations is limited because an acceptable theoretical model of the sources of the main field has not been developed. The change (growth or decay) in the intensity of a secular variation is as large as 150 γ (150 nT) per year (ref. 6). Although this change is nominal in a year's time, the accumulation of several yearly secular changes completely outdates magnetic measurements for a particular epoch, i.e. reference date. Secular variation charts that indicate field changes as a function of time are issued by the U.S. Naval Oceanographic Office.

2.1.3 Temporal Variations

Temporal variations are short duration disturbances in the geomagnetic field resulting from solar activity and changing relative positions of the Sun and Earth. These variations typically have durations ranging from a few seconds to several days and amplitudes from a few hundredths to several hundred gammas.

The frequency of occurrence is determined by the rotation rates of the Earth and Sun. The Sun's rotation can place an active solar area opposite the Earth once every 27 days. These active solar areas may persist for as long as 8 to 10 solar rotations. A semiannual increase in the magnitude of temporal variations occurs during the March-April and September-October periods when the Earth is near the equinoxes.

The intensity of temporal variations is related to the number of sunspots. The number of sunspots in turn changes with the 11-year solar cycle as shown in the prediction in figure 5. Intensity also varies with the type of temporal variation; diurnal, magnetic storm, or sudden impulse disturbance.

Diurnal variations are smoothly changing day-to-night variations in geomagnetic field intensity. The change in any field component caused by diurnal variations is generally less than 200 γ (200 nT) (ref. 10). The characteristics of these disturbances are discussed in section 2.1.4.

Magnetic storms are intervals of magnetic activity that occur almost simultaneously on a worldwide basis. Magnetic storms progress through the characteristic phases illustrated in figure 6 (ref. 3). Occasionally the initial phase is preceded by a preliminary reverse phase which has a duration of a few minutes. The initial or sudden commencement phase has a duration of about one hour during which the total field intensity increases by about 50γ (50 nT). The main phase has a duration of a few hours during which the total field intensity decreases by more than 400γ (400 nT). During the main phase, the horizontal field component has a marked decrease in intensity. The greatest change occurs in the polar regions and can exceed 1000γ (1000 nT). The initial recovery phase has a duration from about six hours to about two days during which time the total field intensity rapidly returns to near pre-storm levels.

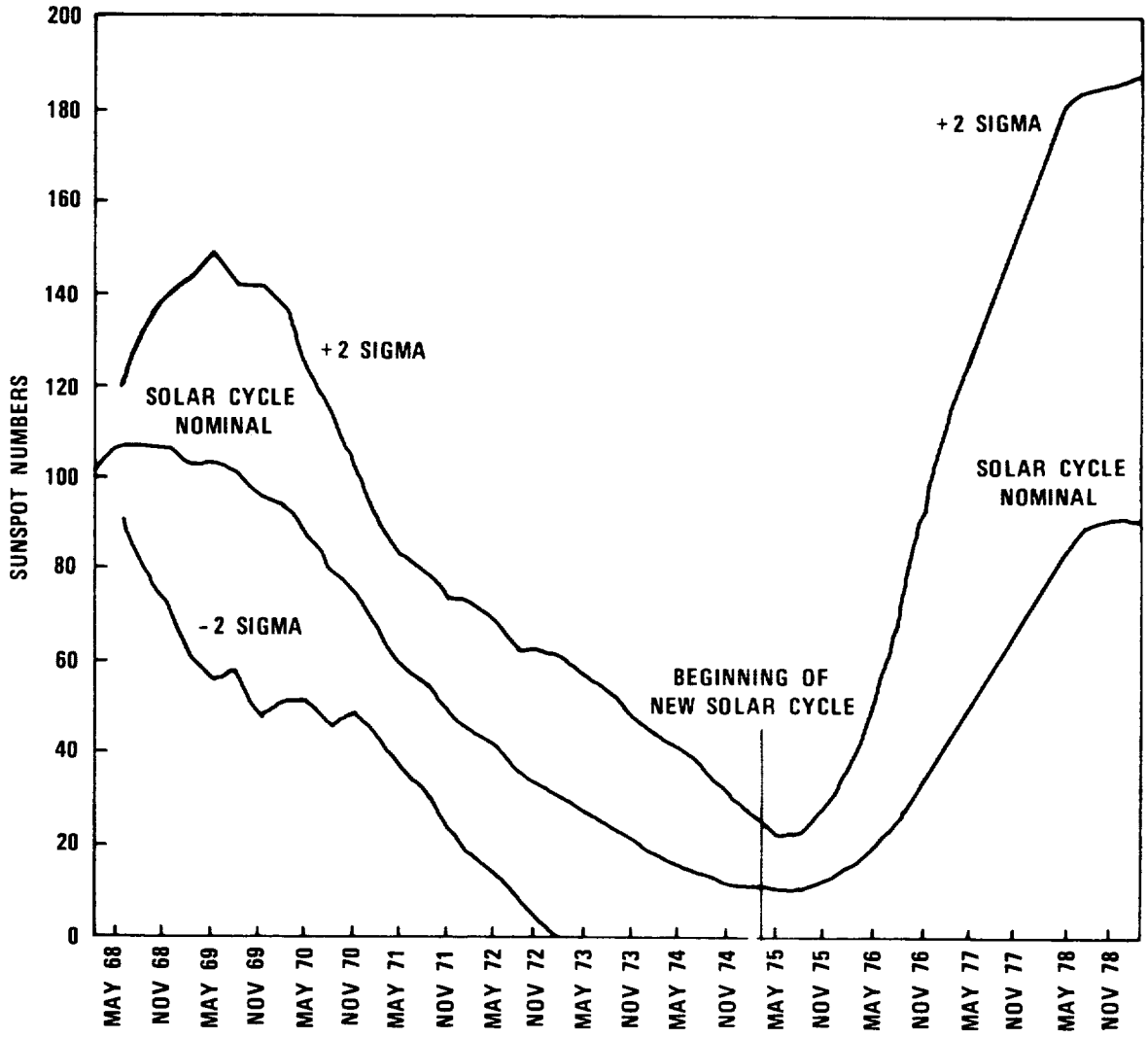

Figure 5.–Predicted sunspot numbers.

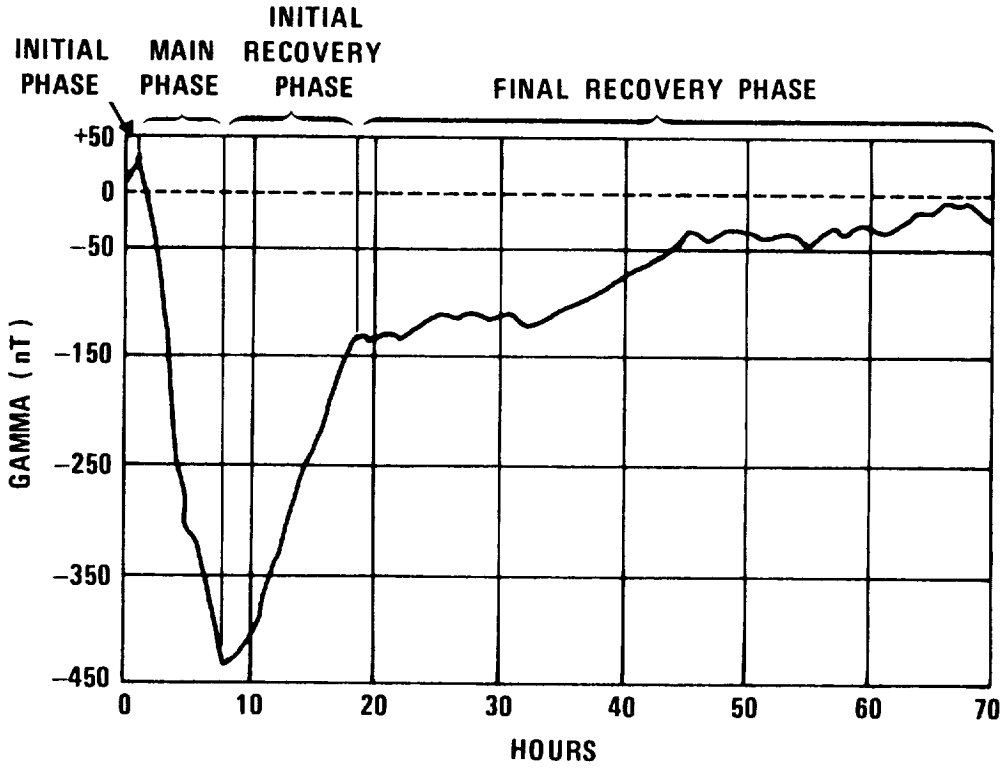

Figure 6.—Magnetic storm effect on main geomagnetic field intensity (observation of a large magnetic storm in Hawaii, February, 1958) (ref. 3).

The change in the surface geomagnetic field resulting from magnetic storms can be as large as 400 γ (400 nT). The final recovery phase has a duration of several days during which time the total field intensity returns to pre-storm levels. The maximum change in the surface geomagnetic field is about 100 to 150 γ (100 to 150 nT). A typical surface field change is about 40 γ (40 nT) (ref. 10).

Sudden impulse disturbances are short duration, low amplitude fluctuations of the geomagnetic field on a worldwide basis as shown in figure 7 (ref. 5). A sudden impulse disturbance has a duration of about one hour or less. Amplitudes as large as $\pm$ 18 γ ($\pm$ 18 nT) have been observed for these disturbances at the Earth's surface.

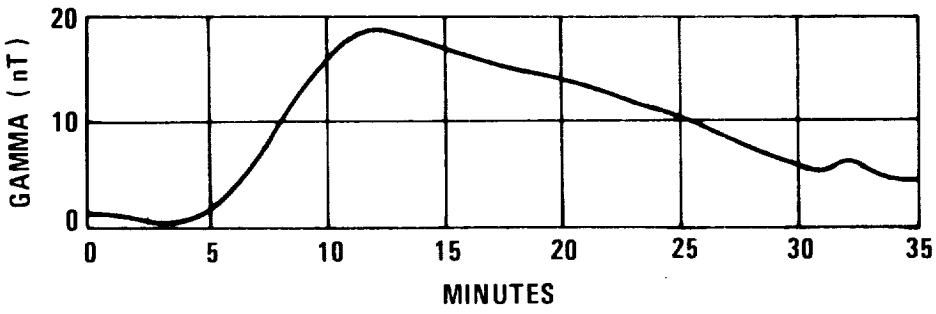

Figure 7. Sudden impulse disturbance (ref. 5).

Very small magnetic field intensity changes which are oscillatory and of short duration are superimposed on the temporal variations described above. These changes are called micropulsations and have periods of less than two or three minutes and amplitudes of less than a few gamma. Micropulsations with a period less than seven seconds and an amplitude less than one γ (1 nT) have been observed (ref. 11).

2.1.4 Ionospheric Currents and Related Disturbances

Ionospheric currents result from systems of charged particles moving between 50 kilometers and the outer reaches of the ionosphere (approximately 600 kilometers) (ref. 9). Changes in ionospheric currents are the main sources of the diurnal variations of the geomagnetic field. Because the intensity of the magnetic field resulting from these currents decreases rapidly with increasing distance, the ionospheric currents do not make significant contributions to the geomagnetic field at distances greater than a few Earth radii, R_e, from the Earth's surface (ref. 12). Those currents which flow perpendicularly to the geomagnetic field lines are most intense near 100 kilometers and those flowing parallel to field lines reach a maximum intensity at approximately 150 kilometers (ref. 11).

2.1.4.1 Auroral Currents

Auroral currents are the polar electrojets and other transient currents associated with aurora and changes in the geomagnetic field. They occur mainly in the polar ionospheric regions above 67° geomagnetic latitude or about 23° from the geomagnetic poles (ref. 9). However, aurora have occasionally occurred in the middle latitudes. Auroral activity has a periodicity that is related to the surface activity of the Sun and its 27-day rotation period. According to reference 11, maximum activity occurs during the spring and fall when the Earth is at the equinoxes. The polar electrojet usually flows westward and encircles the polar region with part of the electrojet crossing the polar cap and rejoining the circular electrojet in the morning sector. Intensity changes in the polar electrojets can cause intense negative geomagnetic bays (polar magnetic substorms whose recorded curve resembles the shape of a

geographical bay in a coastline). Intense negative excursions as great as 2000 γ (2000 nT) have been observed. These excursions as shown in figure 8 (ref. 11) are typically about 1500 γ (1500 nT) and have a duration of about 30 to 120 minutes. An intense negative bay starts in the midnight sector of the electrojet and propagates in all directions.

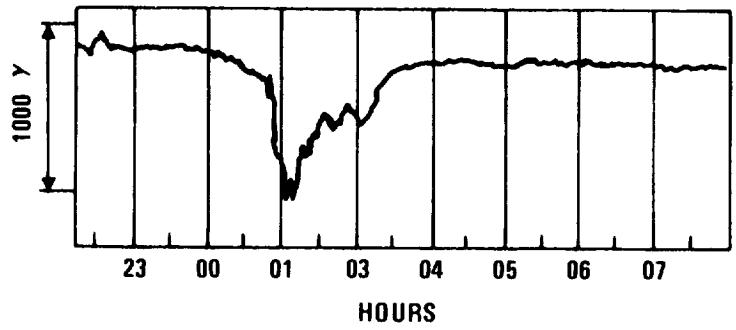

A. Observation at Sitka, Alaska

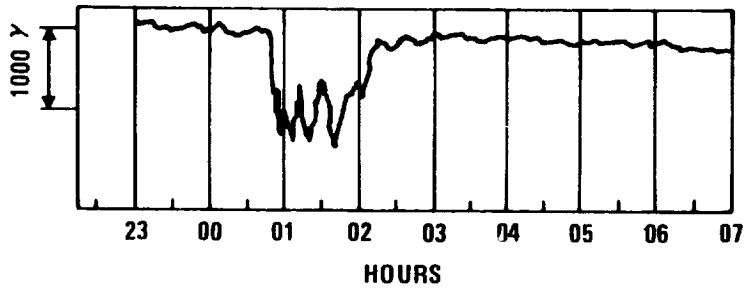

B. Observation at College, Alaska

Figure 8.--Horizontal component of surface geomagnetic field during a polar magnetic substorm (ref. 11).

2.1.4.2 Equatorial Electrojets

The equatorial electrojets are laterally limited, relatively intense currents located in the ionospheric region above the magnetic equatorial zone at an altitude of about 95 to 110 kilometers. They generally flow in a west-to-east direction in the sunlit hemisphere. Observations made during rocket flights indicate the presence of lower and upper current layers. Heppner in chapter V-2 of reference 11 cites Cahill's interpretation of the rocket data as indicating the presence of a west-to-east electrojet about 20 to 25 kilometers above the lower current layer. In the same chapter Heppner cites subsequent research and analysis by Maynard which led him to substanially the same conclusion.

2.1.4.3 Solar Currents

Solar currents in the ionospheric E region are called solar quiet or quiet day solar daily variation (S_q) currents. The daily magnetic variation induced by changes in the S_q currents is described in terms of an average of the 5 days per month that had the least magnetic variation (quiet days) or more commonly in terms of an average of quiet days selected from each month. S_q current systems are formed in the subsolar and antisolar hemispheres. These systems are stationary with respect to the Sun but have a 24-hour period with respect to an observer on the Earth. Increased activity on the Sun's surface causes an increase in the ion density and conductivity of the ionosphere, thus increasing the intensity of the quiet-day variation currents in the subsolar hemisphere. The S_q currents in the middle latitude regions cause variations in the surface geomagnetic field of about 20 to 40 γ (20 to 40 nT). The S_q currents located near the magnetic equator (Huancayo, Peru) cause surface variations of about 100 to 200 γ (100 to 200 nT) (ref. 10).

2.1.4.4 Lunar Currents

Lunar (L) currents in the ionospheric E region are similar to quiet-day variation currents but are only about 1/30 as intense. L currents are generated by the gravitational attraction of the Moon, causing movement of ion masses in the ionosphere. These movements cause variations in the surface geomagnetic field of about 1 γ (1 nT) with a period of 12 hours.

2.1.5 Ring Currents

Ring currents are produced by the movement of electrons and protons in circular spatial distributions within the magnetosphere. The intensity and spatial distribution of ring currents are not well defined and therefore these sources of geomagnetic field variations are not usually included in field calculations (ref. 12).

2.1.6 Magnetic Field at Synchronous Altitude

The equatorial magnetic field at the geocentric distance of about 6.65 R_e consists of the steady-state geomagnetic field plus the temporal variations of this field. On magnetically

quiet days, diurnal magnetic field disturbances due to external field sources cause a 10 to 15% variation in the total magnetic intensity. During magnetic storms, the field at synchronous altitude can increase by 50%, decrease to zero, and even reverse in direction.

Figure 9 shows the intensity of the field components as a function of longitude at synchronous altitude. (These curves are derived from a 24-term spherical harmonic expansion and reflect only that portion of the field due to internal sources.)* The curves are reasonably accurate for magnetically quiet-day conditions along either the dawn or dusk meridian; the values at these meridians differ by about 15%.

Figure 10 (ref. 13) illustrates the diurnal variation of the field components at the longitude of Hawaii on a magnetically quiet day. The vertical and east component showed little variation during the day. The horizontal component has a variation of about $\pm$ 15 γ ($\pm$ 15 nT). The magnetic field intensity is maximum at local noon (2200 hours Greenwich mean time at Hawaii) because of the steady-state compression of the magnetosphere by the solar wind and at minimum intensity at local midnight because of expansion of magnetosphere in the antisolar direction.

Figure 11 (ref. 13) presents field measurements at the longitude of Hawaii made by the ATS-1 synchronous satellite during a magnetic storm on 13, 14 and 15 January 1967. Shortly after local noon on 14 January the magnetopause dipped below synchronous altitude. This event is indicated by the discontinuity in ATS-1 measurements–marked "boundary crossings" on the figure. During a two-hour period the horizontal component of the field reversed in direction with a maximum magnitude of $-140\,\gamma$ (-140 nT) and, within an hour, reached a peak of $+180\,\gamma$ ($+180$ nT). Shortly after local noon of 15 January, magnetic conditions had returned to the typical quiet-day variations.

2.1.7 Cusp Region

The cusp region as shown in figure 1 is located on the antisolar side of the magnetosphere where the dipolar field geometry is transformed into the field geometry of the magnetotail. The cusp region is characterized by a dipolar field, high density of charged particles, and an abrupt change in the magnetic field intensity at the outer boundary as shown in figure 12 (ref. 14). The region is part of the Van Allen radiation belts and is located between about 8 to 16 R_e and within geomagnetic latitudes of about $\pm 25^\circ$. The position of the outer boundary of the cusp region varies daily. This boundary is characterized by abrupt and large changes in particle density, and has a variation in field intensity of the order of 5 to 20 γ (5 to 20 nT) (ref. 14). The magnitude of the magnetic field changes from about 30 γ (30 nT) on the cusp side of the outer boundary to about 15 γ (15 nT) on the magnetotail side of this boundary.

*Computational model of the geomagnetic field is discussed in appendix C.

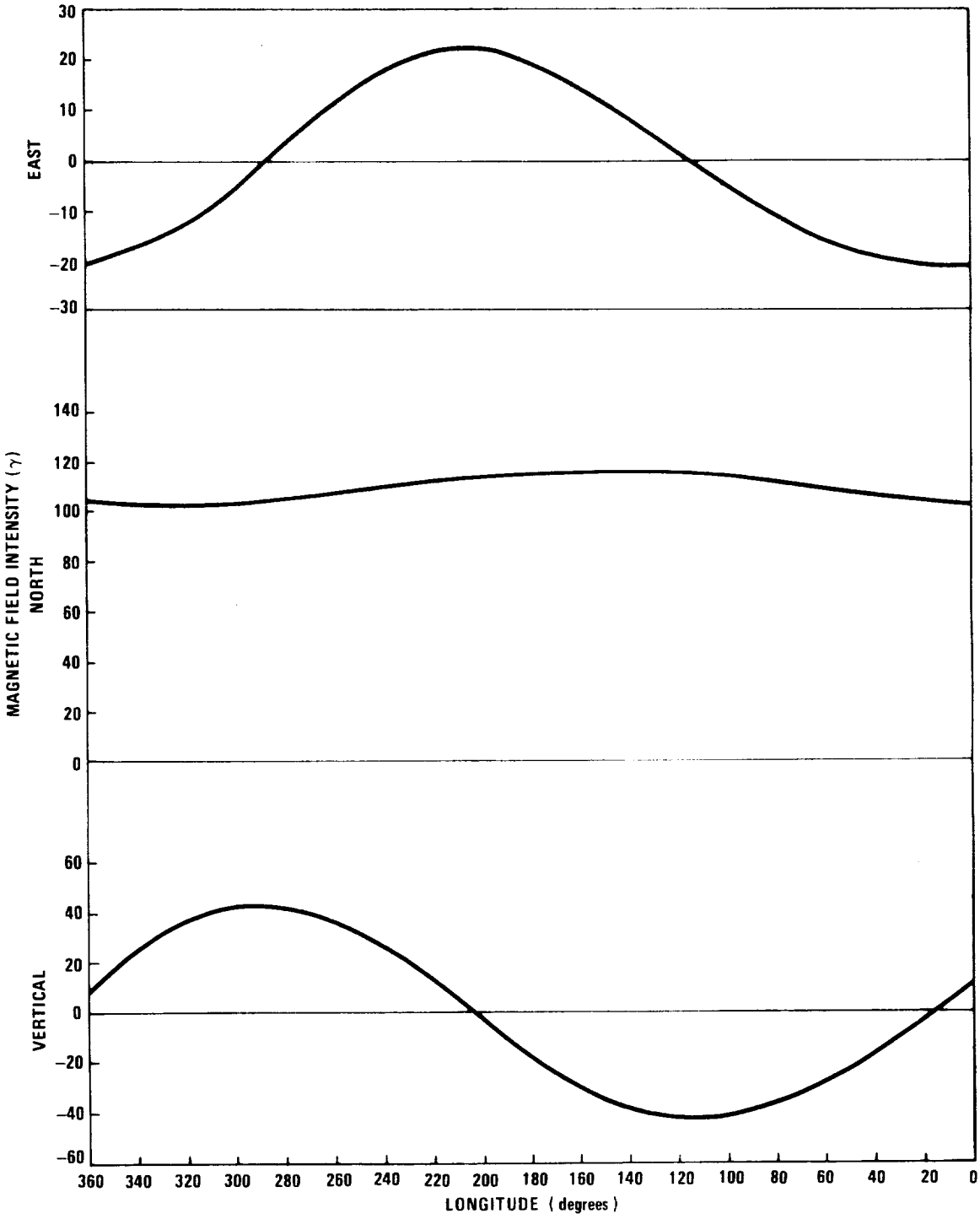

Figure 9.–Magnetic field at synchronous altitude from internal source (Computed from a 24-term harmonic expansion for 3 November 1968).

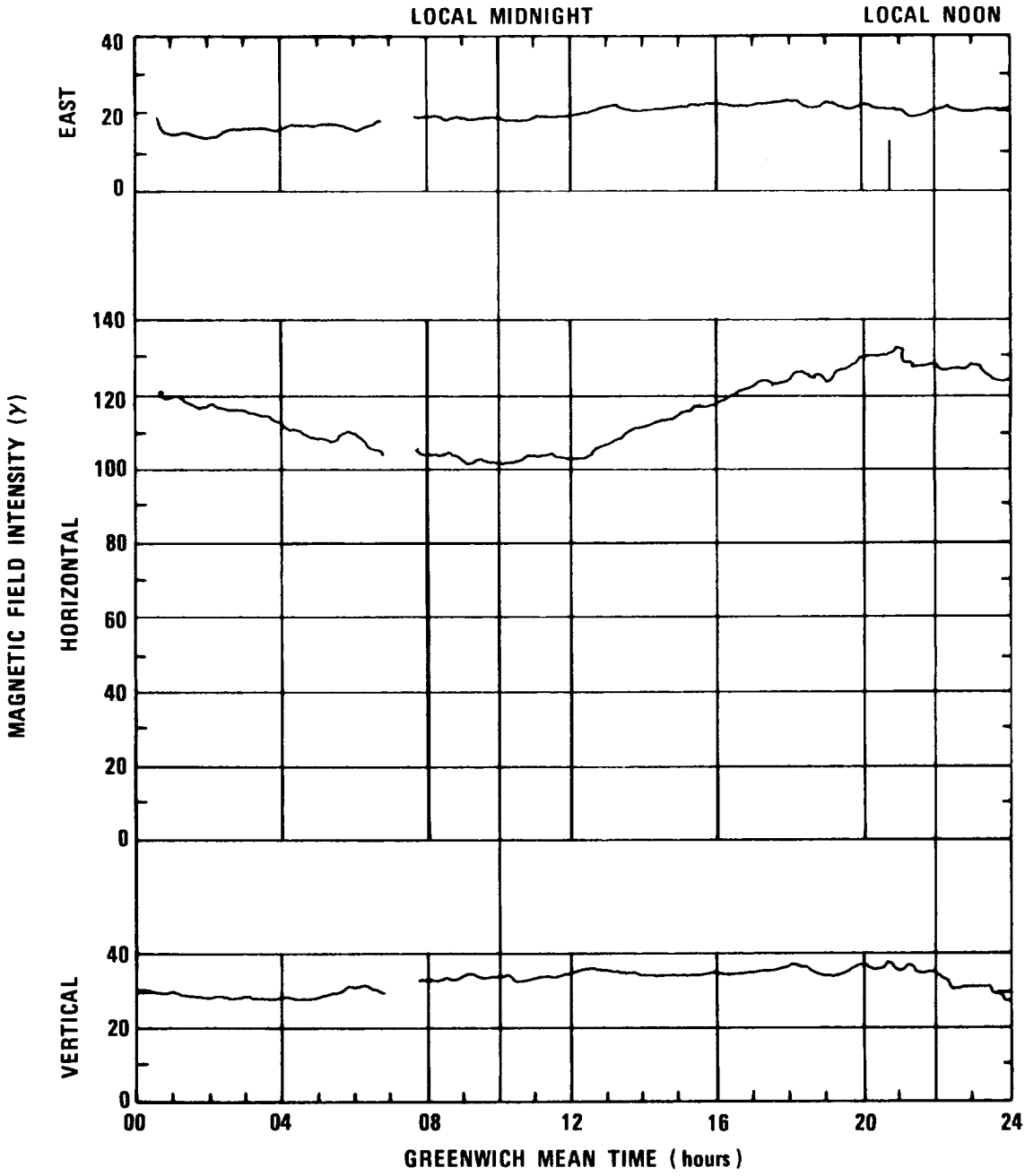

Figure 10.–ATS-1 magnetic field measurements at synchronous altitude showing diurnal variation on 4 January 1967, at 150° west longitude (ref. 13).

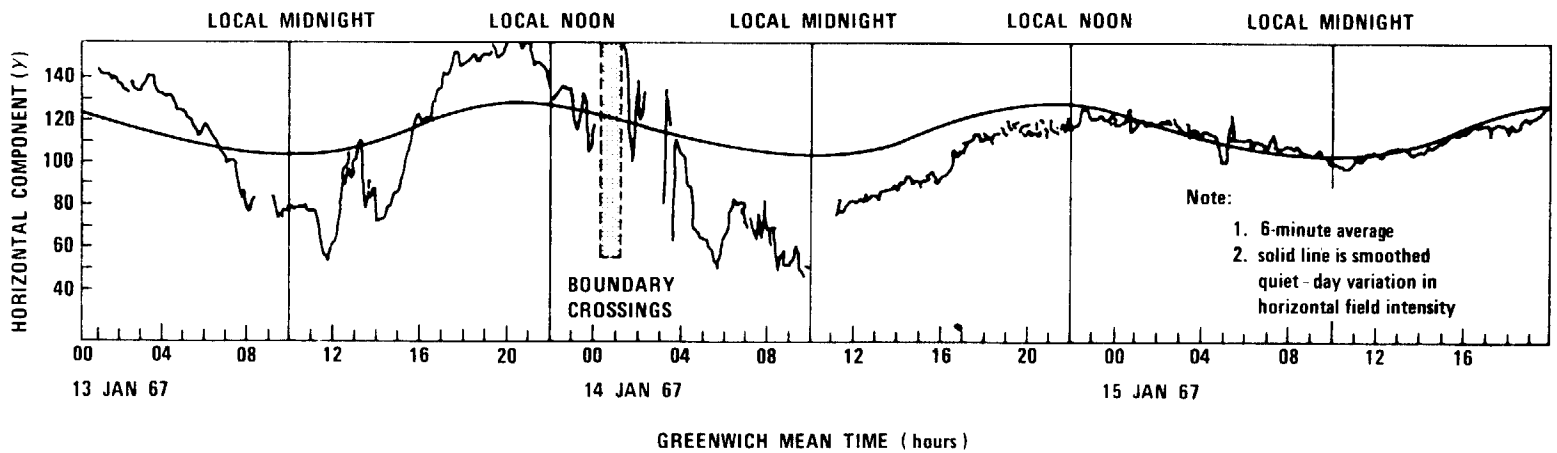

Figure 11.—ATS-1 magnetic field measurements at synchronous altitude showing horizontal intensity variations during a magnetic storm (ref. 13).

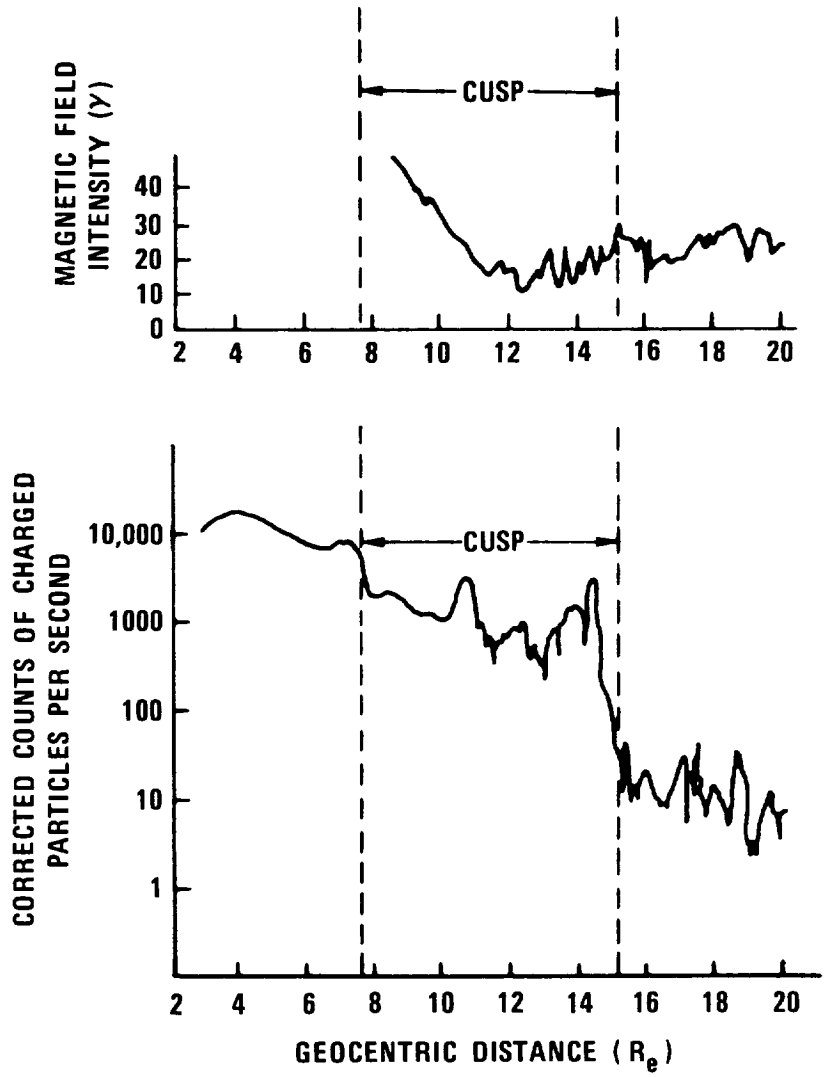

Figure 12.–Observed magnetic field intensity and particle density in cusp region (ref. 14).

2.1.8 Magnetopause

The magnetopause as shown in figure 1 is the boundary layer that separates the relatively strong geomagnetic field from the magnetosheath. This boundary layer has hourly and daily displacements of 1 to 3 R_e but generally extends from about 10 R_e at the subsolar side to at least 80 R_e on the antisolar side of the magnetosphere (ref. 15). During a magnetic storm, the changes in the interplanetary magnetic field and in solar wind intensity cause the magnetopause to expand or contract at rates greater than 50 km/sec (ref. 13).

The magnetopause is a barrier region some tens of km in thickness in which the magnetic field intensity is low and the magnetic field direction shifts by as much as 180 degrees. The magnetopause is the transition zone from field intensities greater than 40 γ (40 nT) in the magnetosphere to field intensities of about 10 to 30 γ (10 to 30 nT) in the magnetosheath as shown in figure 13 (ref. 16).

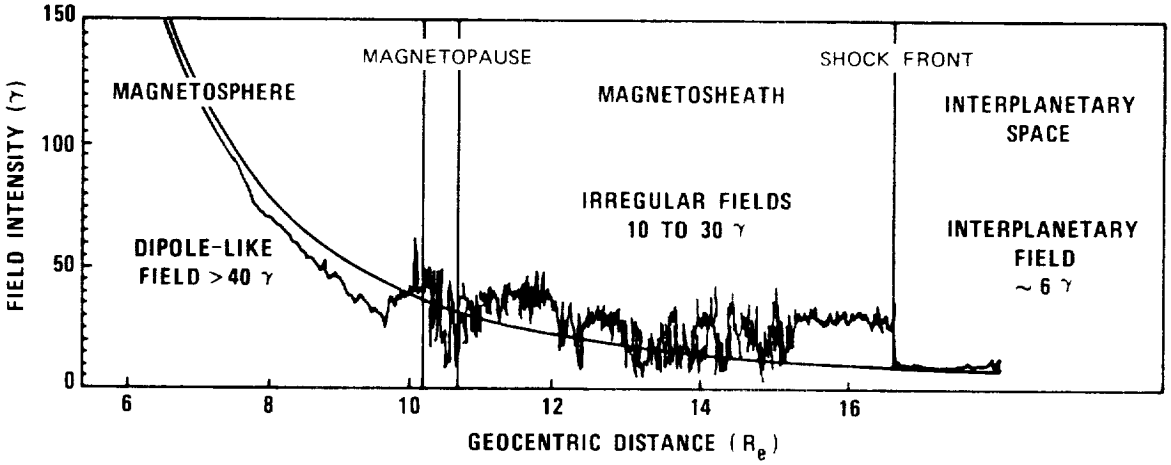

Figure 13. Magnetic field intensity in magnetosheath from Mariner V observations (ref. 16).

2.1.9 Magnetosheath

The magnetosheath, as shown in figure 1, is the transition zone in which the interplanetary field and the solar wind are deflected after passing through the shock front. In this region, the weak interplanetary field is compressed and deflected. The field compression increases the magnetic field intensity in the magnetosheath to a nominal 10 to 30 γ (10 to 30 nT) as shown in figure 13 (refs. 16 and 17), however, during intense magnetic storms the field has exceeded 100 γ (100 nT). The magnetosheath field intensity is also characterized by rapid oscillations with periods of 4 to 15 seconds and with 2 to 5 γ (2 to 5 nT) peak-to-peak amplitudes (ref. 18).

The thickness of the magnetosheath in the Earth-Sun direction is a nominal 4 R_e; it can shrink to about 2 $\pm$ 0.5 R_e during a magnetic storm that occurs during a year of low solar activity. As any magnetic storm activity decreases, the magnetosheath increases to its nominal thickness (ref. 15).

2.1.10 Shock Front

The shock front, as shown in figure 1, is the outermost boundary of the magnetosheath and is created by the interaction of the solar wind with the geomagnetic field. Observations made at the shock front indicate the presence of large amplitude magnetic field oscillations of 10 to 50 γ (10 to 50 nT) as shown in figure 14 (ref. 18). On the magnetosheath side of the shock front, erratic and periodic oscillations occur with amplitudes of 2 to 5 γ (2 to 5 nT) and periods of about 4 to 15 seconds. At the shock front, higher frequency oscillations occur with amplitudes ranging from 5 to 10 γ (5 to 10 nT) and frequencies on the order of 1 to 3 Hz and higher (ref. 19). On the interplanetary side of the shock front, oscillations have been known to occur with amplitudes of 2 to 5 γ (2 to 5 nT) and periods of about 20 to 60 seconds (ref. 18).

2.1.11 Magnetotail

The magnetotail, as shown in figure 1, is formed by the solar wind sweeping back the geomagnetic field lines in the antisolar direction. Magnetotail field lines from southern hemisphere are predominantly directed in an antisolar direction and separated by the neutral sheet from field lines from northern hemisphere, which are predominantly solar directed. Pioneer VII observations indicate that the magnetotail extends to at least 1000 R_e, and IMP-1 observations indicate that it has a radius of about 20 R_e at a geocentric distance of 30 R_e (refs. 14 and 20). Direction of the field in the magnetotail is generally close to the plane of the ecliptic and at a solar coordinate angle ϕ_{SE} between 270° and 360° (ref. 21).*

*Solar ecliptic coordinates are defined in appendix A.

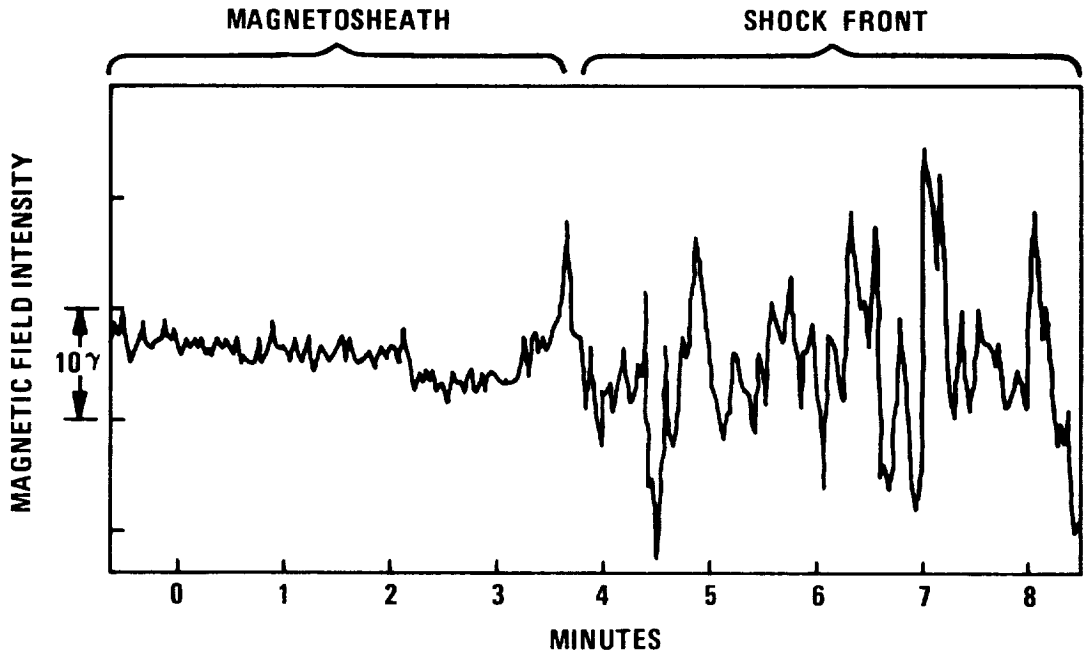

Figure 14. Observed magnetic field oscillations at shock front (ref. 18).

The configuration of the magnetotail is well defined to a geocentric distance of about 80 R_e. At distances of 500 to 1000 R_e the configuration appears to be characterized by separate tubes of magnetic filaments (ref. 22).

The magnetic field intensity in the magnetotail to a geocentric distance of about 8 to 10 R_e decreases at a rate expected for the Earth's dipolar field.* Beyond 10 R_e, Explorer 33 observations in the magnetotail indicate that the field intensity generally decreases as distance from the Earth increases. This decrease is from about 20 γ (20 nT) at 10 R_e to about 7 γ (7 nT) at 80 R_e. Between 10 R_e and 30 R_e, IMP-1 observations indicate that the median field intensity is about 16 γ (16 nT) (ref. 22). Ness (ref. 4) indicates that from 20 R_e to 60 R_e, a decrease from about 16 to 8 γ (16 to 8 nT) is to be expected. Pioneer VII observations indicate that the field intensity is generally between 4 and 16 γ (4 and 16 nT) at about 1000 R_e. The currents within the neutral sheet cause magnetic field depressions that extend northward and southward from the neutral sheet to a distance of about 5 R_e and may extend lengthwise along the neutral sheet for distances greater than 15 R_e.

*See presentation of dipolar model in appendix C.

2.1.12 Neutral Sheet

The neutral sheet, as shown in figure 1, is a region within the magnetotail where abrupt reversal of the magnetic field from the solar to the antisolar direction occurs and in which magnetic intensity decreases to a low value. The neutral sheet extends from about $10 \pm 3\ R_e$ to $1000\ R_e$ or to the limit of the magnetotail (ref. 23). The sheet is approximately parallel to the solar-magnetospheric equatorial plane* with a position above the plane during summer months and below the plane during winter months (ref. 23). During a magnetic storm, the front boundary of the neutral sheet has been observed to be displaced to geocentric distances beyond $13\ R_e$, returning to about $10\ R_e$ as storm activity decreases (ref. 24).

The magnetic field intensity in the neutral sheet is about 1 to 4 γ (1 to 4 nT) on the dawn meridian side and less than 1 γ (1 nT) on the side near the noon-midnight meridian plane. The thickness of the neutral sheet varies from about 500 km to about 5000 km.

2.2 Models of the Earth's Main Field

The analytical models of the Earth's main (geomagnetic) field discussed in this monograph represent an undistorted, steady-state field and do not account for the effects of external sources or localized Earth anomalies. An analytical model that considers some external sources has been developed by Mead (ref. 12), but it is a simplified model.

2.2.1 Spherical Harmonic Expansion Model

The spherical harmonic expansion model of the geomagnetic field is based on a series expansion in spherical coordinates of the geomagnetic potential devised by Gauss in the 1830's and which satisfies LaPlace's and Maxwell's equations.** The accuracy of this model derives from the use of a large number of coefficients in the harmonic expansion. Cain Hendricks, Langel, and Hudson (ref. 25) proposed an expansion of 120 coefficients with associated first and second time derivatives for use with the model for the "International Geomagnetic Reference Field – 1965." With these coefficients, the model has expected maximum errors of the order of a few tens of gammas in total field intensity at the Earth's surface (except for Antarctic regions). At satellite altitudes of about $4\ R_e$, errors are reduced by a factor of 3 to 4, but at higher altitudes the effects of external sources increase so that the model gradually becomes less representative of the actual environment, particularly beyond $6.6\ R_e$ (synchronous altitude).

The spherical harmonic expansion model of Cain, et al. is currently considered the best analytical representation of the geomagnetic field and has been adopted

* Solar magnetospheric coordinates are defined in appendix A.

** Analytical presentation of field models is in appendix C.

for this monograph. The abbreviated versions of this model discussed in 2.2.2 and 2.2.3 are less accurate but often useful for quick estimates of the field.

2.2.2 Quadrupole Model

The quadrupole model of the geomagnetic field is derived by using the first eight terms of the spherical harmonic expansion model. This model includes both dipolar and quadrupolar effects. At geocentric distances greater than 1.2 R_e, the maximum error between computed and actual fields is about 20% in magnitude and 10° in direction. At distances less than 1.2 R_e, the error increases until it reaches about 40% in magnitude and 20° in direction at the Earth's surface.* This large error is caused by deviation of the Earth's surface field from a dipole or quadrupole field. Figure 15 (ref. 26) illustrates the magnitude and angular deviations of the quadrupole model as a function of geocentric distance.

2.2.3 Dipole Models

The spin-axis dipole model of the geomagnetic field is derived by using the first term of the spherical harmonic expansion model. This model corresponds to a magnetic dipole located at the Earth's center with its magnetic poles aligned to the Earth's spin axis. The spin-axis dipole model yields field magnitudes that are generally lower than the actual field; this model is the least accurate of the models of the geomagnetic field.*

The tilted dipole model is obtained by using the first three terms of the spherical harmonic expansion model. This model has the dipole's axis tilted away from the Earth's spin-axis by 11.44° so that magnetic North Pole is near Thule, Greenland. At geocentric distances greater than 3 R_e, solar wind and solar plasma effects cause the actual magnetic field to be significantly different from the computed tilted dipole field. At 3 R_e, maximum errors are about 9% in magnitude and 7° in direction. At distances less than 3 R_e, magnitude errors may be as great as 40 to 60%.* Figure 15 illustrates the magnitude and angular deviations of the tilted dipole model as a function of geocentric distance.

2.3 Interplanetary Field

The interplanetary field is the Sun's magnetic field which is represented as a sectionalized, spiral field. This field extends radially from the solar photosphere for a few Sun radii and then begins to form into a spiral as shown in figure 16 (refs. 27, 28 and 29). Beyond several solar radii (outside the region indicated by the dashed circle in figure 16) the rotational interaction causes the interplanetary field to form into an Archimedes spiral. The field polarity varies with the sectors, a sector of one polarity often being as large as 180°. IMP-1 detected four sectors of alternating polarity as shown in figure 16. The interplanetary field

*Analytical presentation and accuracy comparison of field models are in appendix C.

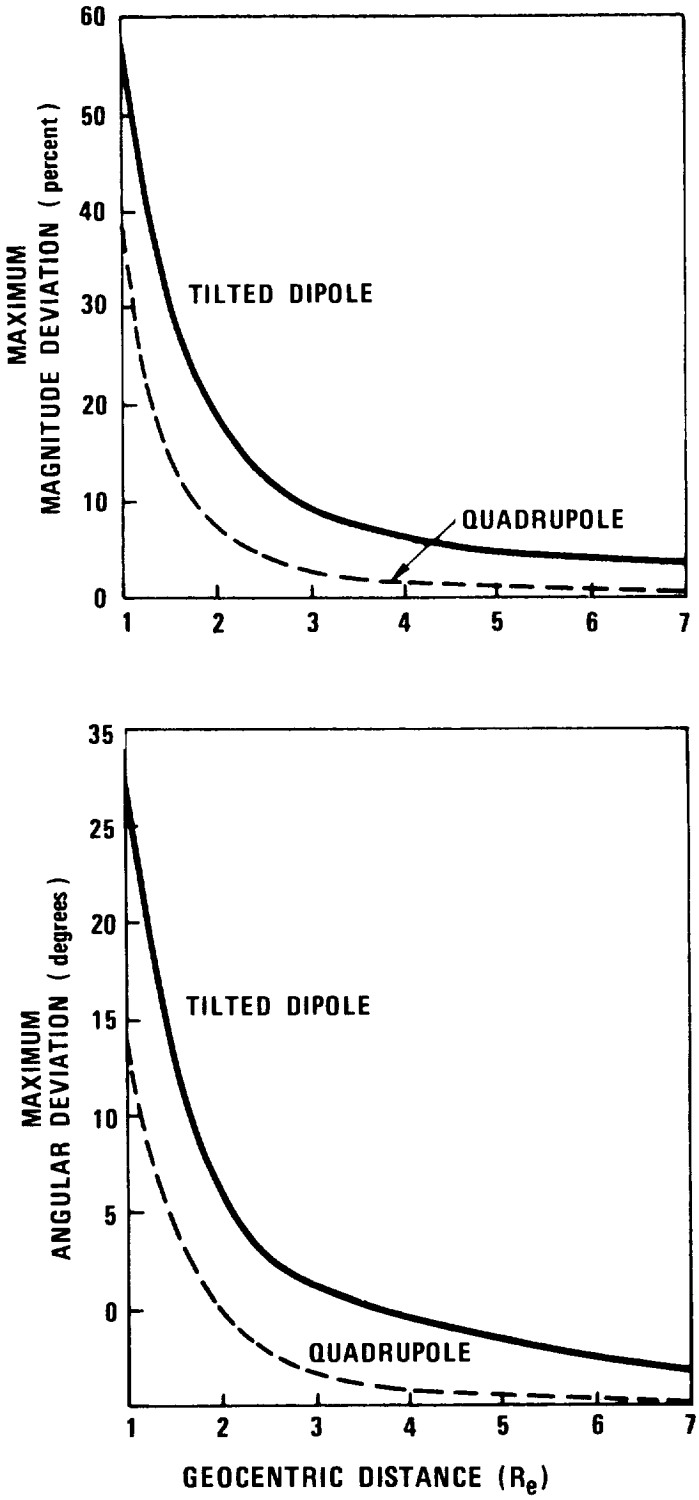

Figure 15.- Maximum deviations of quadrupole and tilted-dipole models from spherical harmonic expansion model (ref. 26).

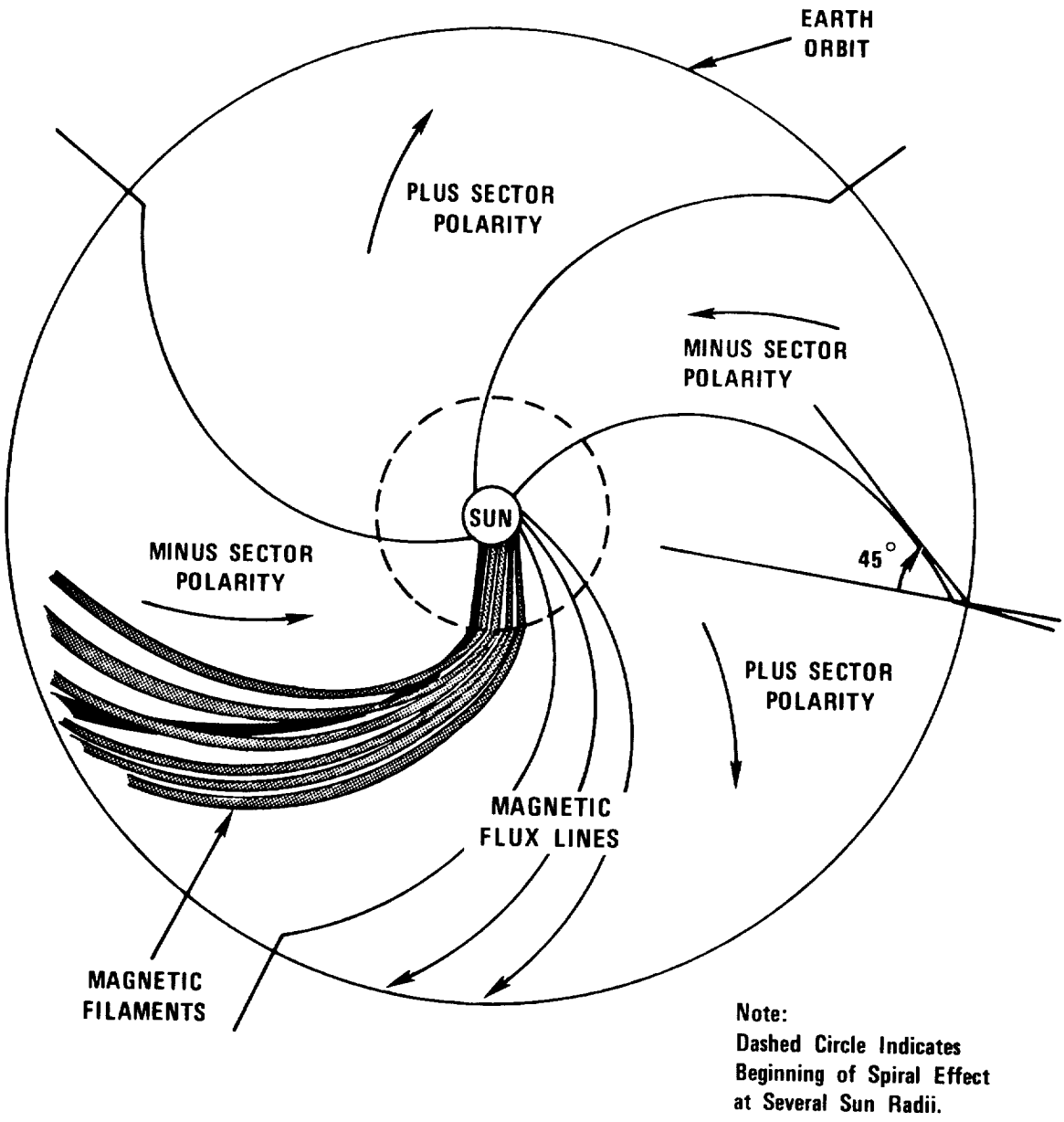

*Figure 16.–Sample structure of interplanetary field (refs. 27, 28, and 29).

intersects the Earth's orbit in the plane of the solar equator (about 7° from plane of ecliptic) at an angle of about 45° to the Earth-Sun line as illustrated in figure 16 when the solar wind velocity is 450 km/sec (ref. 28). Microstructure in the interplanetary field is the source of magnetic fluctuations of less than one-hour duration which are characterized by shock waves and plasma-magnetic field discontinuities. Mesostructure field effects produce magnetic variations of about 1 to 100 hours and are characterized by magnetic filaments (tubular groupings of lines of force) and low-frequency magnetohydrodynamic waves. Macrostructure field effects produce magnetic variations of over 100-hour duration and are characterized by sectoring and very wide magnetic filaments (ref. 30), as illustrated in figure 16, with diameters of an order of 3×10^6 km. Pioneer VI observations provide evidence of the existence of magnetic filaments and also indicate that they are sometimes intertwined and corotate with Sun. The rotating sector structure and polarity of the interplanetary field has been increasingly studied in recent years. Satellite measurements in the vicinity of 1 A.U. have been extrapolated in the ecliptic plane to obtain mapping of the field between 0.4 and 1.2 A.U. (ref. 31). A solar flare can send an intense magnetic disturbance propagating outward into the interplanetary field disrupting its structure. After the disturbance, a new structure forms that is very similar to the preceding one.

The magnitude of the interplanetary field in the vicinity of the Earth is fairly constant with a nominal value of about 6 γ (6 nT) and a range of 2 to 40 γ (2 to 40 nT) (ref. 30). At the Sun's equator and outside of active centers the solar magnetic field intensity is estimated at about 40 gauss (.0004 T). An average interplanetary intensity of 2 γ (2 nT) implies that the magnetically active region of the photosphere has a magnetic field intensity of about 100 gauss (.01 T) (ref. 29).

Large amplitude disturbances of the interplanetary field are associated with transient solar features which occur in centers of local activity. Strong magnetic fields are characteristic of sunspots, occasionally reaching 3000 gauss in a center (ref. 15). The polarity of the lead spots (in the sense of rotation, that is, west) reverse with an 11-year period and the sun's main field reverses with 22-year periodicity (ref. 32).

2.4 Magnetic Fields of Planets and Their Natural Satellites

Spacecraft magnetometer observations have provided upper bounds on the dipole moments of Venus, Mars, and the Moon. Radio observations show that Jupiter has a strong magnetic field, and modulation of decameter emissions indicate that its satellite Io may also have magnetic effects (ref. 33). There have been no observations yielding positive evidence for existence of magnetic fields for the planets Mercury, Saturn, Uranus, Neptune, and Pluto nor any associated natural satellites.

2.4.1 Venus

Spacecraft observations indicate either that Venus has no magnetic field or that it has a field of the same order as the interplanetary field. Mariner V observations indicate an

interplanetary field intensity of about 8 γ (8 nT) near the orbit of Venus and an upper limit of the magnetic dipole moment for Venus of about 10^{-3} times the Earth's dipole moment*, implying that Venus' magnetic field at the equator is less than 35 γ (35 nT). Figure 17 (ref. 16) illustrates the interaction of the solar wind and Venus. In this concept, the solar wind plasma flows around Venus leaving a cavity behind the planet. Mariner V observations indicate a shock front bounding a region similar to Earth's magnetosheath. The solar wind plasma behind the shock front is bounded by an anemopause which is about 50 km above the surface. The anemopause is the interaction layer between Venus' atmosphere and the solar wind. The expansion fan illustrated in figure 17 could be formed by solar plasma expanding into the cavity behind Venus with a rarefaction expansion wave moving away from the cavity in reaction to the inward plasma flow (refs. 16 and 34).

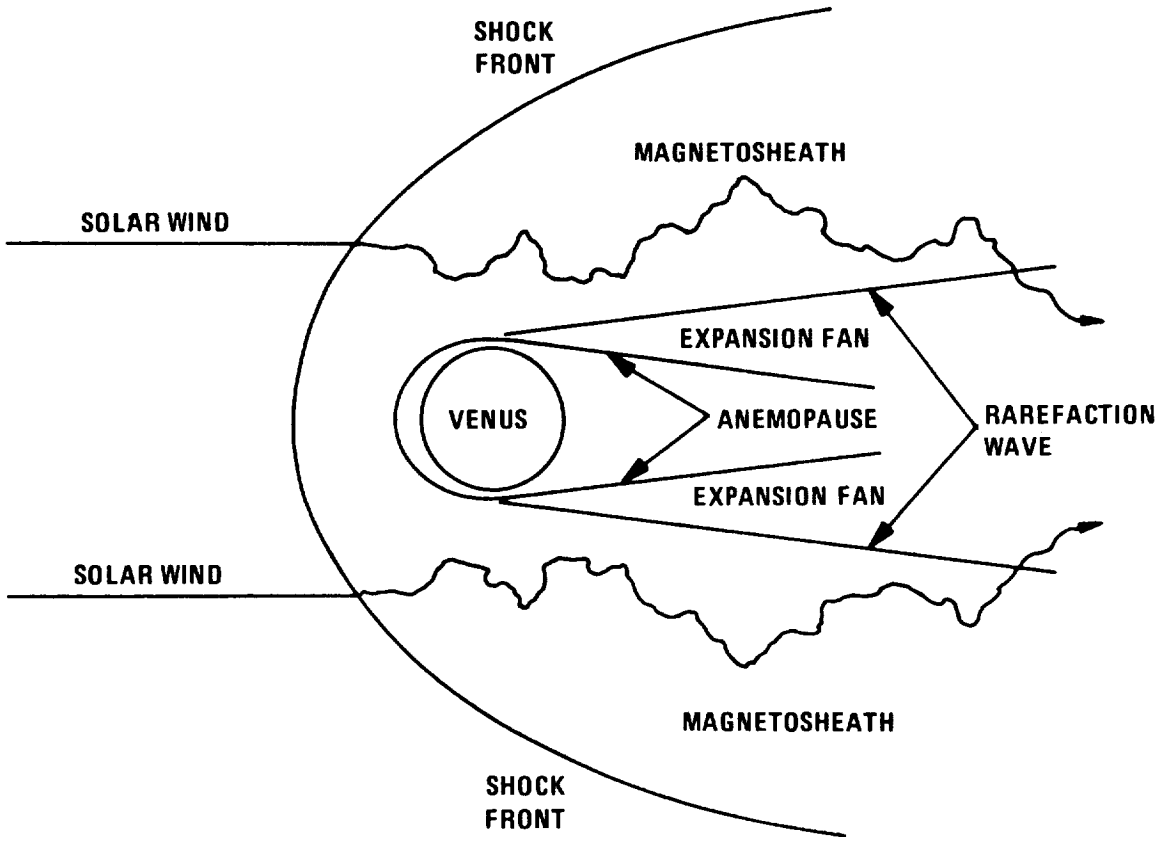

Figure 17.—Interaction model of solar wind and Venus (ref. 16).

*7.99×10^{25} pole-cm (10.04×10^{16} weber-meter) is Earth's magnetic moment.

2.4.2 Mars

Observations made by Mariner IV at 3.9 Mars radii from the center of the planet indicate that no definite effect could be attributed to a Martian magnetic field. Citing these observations, Smith (ref. 35) estimates the Martian magnetic moment to be less than 10^{-4} times Earth's magnetic moment.* A magnetic moment of that order implies a Mars surface magnetic field of about 100γ (100 nT). If Mars has a negligible magnetic field, the solar wind interaction with Mars may be similar to the Venus interaction. However, the magnetic field of Mars may be strong enough to form a magnetosphere with a structure similar to the Earth's magnetosphere (ref. 16).

2.4.3 Jupiter

Jupiter is expected to have a magnetosphere very similar to that of the Earth and extending about 40 to 50 Jupiter radii along Sun-Jupiter line as shown in figure 18 (refs. 16 and 36). Observations of radio emissions from the planet indicate that its magnetic field is at least 10 times as intense as Earth's (ref 4). Smith (ref. 16) reports the estimated value of the surface field to be about 5 gauss (.0005 T). Jupiter's magnetic field resembles a magnetic dipole field with its axis apparently displaced off the planetary center and tilted at 9° or 10° to the axis of rotation; the magnetic polarity is opposite that of Earth's dipole field (ref. 37). Because of a short rotation period (less than 10 hours) conjunctive with a suspected massive, fluid, conducting center, Jupiter's magnetic moment is expected to be greater than the Earth's by as much as a factor of 10^4* (ref. 16).

2.4.4 Saturn

Observations of possible decameter radio emissions from Saturn indicate that this planet may have a moderately strong magnetic dipole moment (ref. 38). In every case the weakness and uncertainty of the radiation defy positive identification. Thus if Saturn is a source of nonthermal radio emissions, the output is far less frequent and much less intense than that from Jupiter. Further observations are required, but Saturn, with its similarity in size and appearance to Jupiter, may have a strong magnetic field whose configuration may be influenced by the presence of Saturn's rings (ref. 39).

2.4.5 Moon

Measurements indicate that Moon's surface magnetic field is less than 8 γ (8 nT) and magnetic moment is less than 10^{-5} times the Earth's magnetic moment* (ref. 40). Explorer 35 data indicates that a lunar shock front does not exist and that the interplanetary field is not significantly distorted by the Moon as shown in figure 19 (ref. 16). Without a shock front, the Moon probably absorbs the solar wind plasma that strikes it with very few particles being deflected.

*7.99×10^{25} pole-cm (10.04×10^{16} weber-meter) is Earth's magnetic moment.

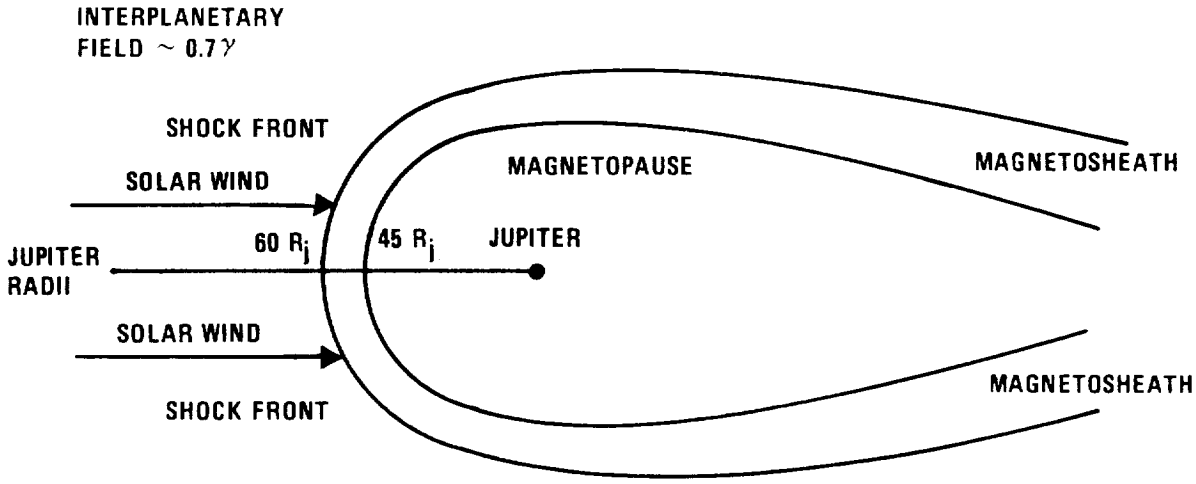

Figure 18.–Magnetosphere of Jupiter (refs. 16 and 33); an idealized schematic cross-section in the ecliptic plane.

The Moon's wake region is characterized by a solar wind umbra and penumbra. Wang (ref. 41) predicts a long non-axial, symmetrical wake behind the Moon (the plane of symmetry is defined by the local solar wind velocity and the interplanetary field direction). The interplanetary field in the solar wind umbra increases about 3 γ (3 nT) with a relative decrease of about 4 γ (4 nT) observed on either side of the increase. The penumbra is characterized by decreases in the interplanetary field which are externally bounded by increases in field intensity (ref. 41).

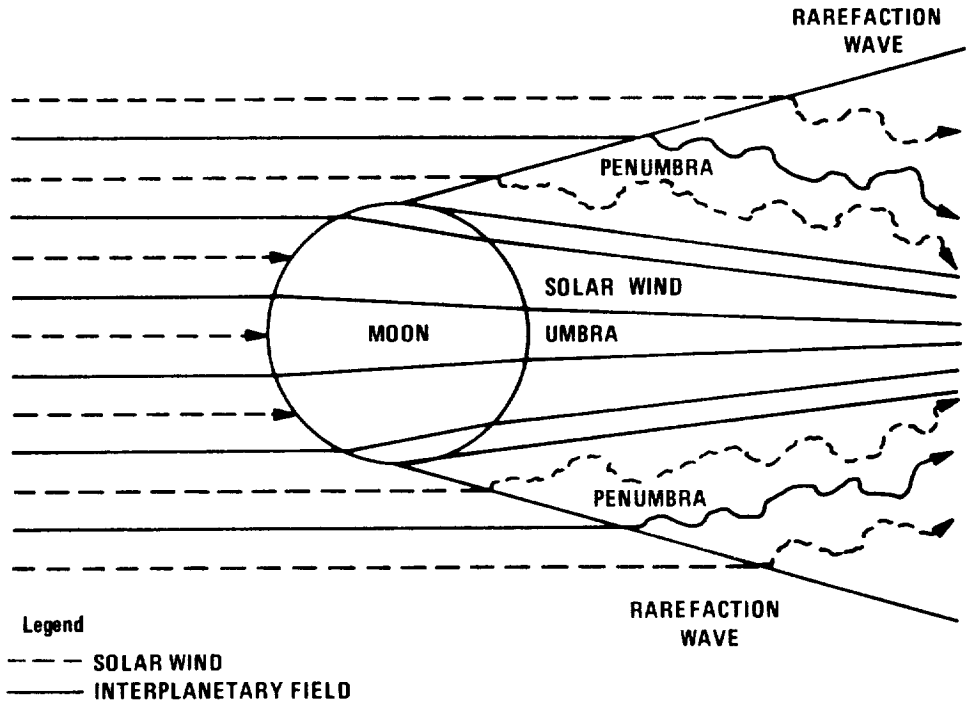

Figure 19. Interaction model of solar wind and Moon (ref. 16).

3. CRITERIA

The analytical models and descriptions of the magnetic fields presented here should be used in the design of space vehicles, space vehicle systems, and the experiments and instrumentation for space applications.

3.1 Earth's Surface

The surface geomagnetic field for the geographical region of interest may be obtained from magnetic charts issued by the U.S. Naval Oceanographic Office, Washington, D.C. 20390 (ref. 8). Figure 3 is a simplified version of one such chart showing the total magnetic field intensity at the Earth's surface.

3.2 Earth's Surface to Synchronous Altitude

The magnetic field environment from the Earth's surface to synchronous altitude (geocentric distance of 6.6 R_e) can be described for most design purposes by the spherical harmonic expansion model (appendix C).

3.2.1 Secular Variations

Secular variations can be as large as 150 γ (150 nT) per year. These variations are included in the spherical harmonic expansion model (appendix C).

3.2.2 Temporal Variations

Temporal variations are not included in the spherical harmonic expansion model but should be considered if these variations could significantly affect a spacecraft's instrumentation or scientific experiments. Expected field changes for temporal variations are as follows. Diurnal variations are generally less than 200 γ (200 nT). Variations caused by magnetic storms vary from about a 50 γ (50 nT) increase at the surface during the sudden commencement phase to a greater than 400γ (400 nT) decrease at the surface during main phase (the time sequences and durations of the phases are described in 2.1.3). Sudden impulse variations are $\pm$18 γ ($\pm$18 nT) maximum at the surface. Micropulsations cause a variation in the field of a few γ (nT) at the surface.

3.2.3 Ionospheric Currents

Magnetic field changes caused by ionospheric currents are less than 2000 γ (2000 nT) and do not make significant contributions to the main geomagnetic field except at geocentric distances below about 2 to 3 R_e.

3.2.3.1 Auroral Currents

Auroral currents (polar substorm) can cause field changes as large as 2000 γ (2000 nT), but the average is about 1500 γ (1500 nT) with a duration of 30 to 120 minutes.

3.2.3.2 Solar Currents

At the Earth's surface, S_q currents can cause field changes in the middle latitudes of 20 to 40 γ (20 to 40 nT). The magnitude of this change increases to 100 to 200 γ (100 to 200 nT) near the magnetic equator.

3.2.3.3 Lunar Currents

At the Earth's surface, lunar currents cause insignificant changes of about 1 γ (1 nT) with a 12 hour period.

3.3 Synchronous Altitude

At synchronous altitude, an average magnetic field of about 138 γ (138 nT) is to be expected. Approximations to the magnetic field in this region may be obtained from the spherical harmonic expansion model (appendix C), but expansion beyond the first 33 terms in this model is not warranted because contributions from external sources are not included. The field at synchronous altitude is highly variable during a magnetic disturbance with increases of 50 percent, decreases to zero, and even reversals of direction (see 2.1.6).

3.4 Beyond Synchronous Altitude

At distances between 6.6 and about 10 R_e, the spherical harmonic expansion model (appendix C) will give an approximation to average quiet day conditions but diurnal and temporal effects in this region are of major significance. Because of the limited applicability of the spherical harmonic model in this region, computations using more than about 20 terms are not warranted. About 10 R_e and beyond, distortions in the geomagnetic field cause deviations from the spherical harmonic expansion model; therefore, estimates of the magnetic field are given for the following regions.

3.4.1 Cusp

The cusp region is part of the Van Allen radiation belts and is located on the night side of Earth between about 8 to 16 R_e and within geomagnetic latitudes of about $\pm 25^\circ$. The cusp region is characterized by dipolar field geometry and an abrupt and large change in particle

density and field intensity at its outer boundary. The magnitude of the magnetic field throughout the cusp region is not well known, but it changes from about 30 γ (30 nT) near its outer boundary to about 15 γ (15 nT) on the magnetotail side of this boundary.

3.4.2 Magnetopause

The magnetopause is the transition zone from field intensities greater than 40 γ (40 nT) in the magnetosphere to field intensities of about 10 to 30 γ (10 to 30 nT) in the magnetosheath. This transition zone or boundary layer is about 100 km thick and has hourly and daily displacements of as much as 1 to 3 R_e but generally bounds the magnetosphere from about 10 R_e on the subsolar side to at least 80 R_e on the antisolar side.

3.4.3 Magnetosheath

The magnetic field intensity in the magnetosheath is a nominal 10 to 30 γ (10 to 30 nT), but during intense magnetic storms, the field intensity has exceeded 100 γ (100 nT). The magnetosheath is characterized by rapid field oscillations with periods of 4 to 15 seconds and with 2 to 5 γ (2 to 5 nT) peak-to-peak amplitudes as well as by periodic and incoherent noise components. The thickness of the magnetosheath in the Earth-Sun direction is a nominal 4 R_e but can shrink to about 2 ± 0.5 R_e during a magnetic storm that occurs during a year of low solar activity.

3.4.4 Shock Front

Observations at the shock front indicate the presence of large amplitude magnetic field oscillations of 10 to 50 γ (10 to 50 nT). On the magnetosheath side of the shock front, erratic and periodic oscillations occur with amplitudes of 2 to 5 γ (2 to 5 nT) and periods of about 4 to 15 seconds. At the shock front, higher frequency oscillations occur with amplitudes ranging from 5 to 10 γ (5 to 10 nT) and frequencies on the order of 1 to 3 Hz and higher. On the interplanetary side of the shock front, oscillations occur with amplitudes of 2 to 5 γ (2 to 5 nT) and periods of 20 to 60 seconds.

3.4.5 Magnetotail

The magnetic field intensity in the magnetotail to a geocentric distance of about 8 to 10 R_e decreases at a rate expected for the Earth's dipolar field. From about 10 to 80 R_e, the field decreases from about 20 γ (20 nT) to about 7 γ (7 nT). Between 10 R_e and 30 R_e, the median field intensity is about 16 γ (16 nT). From 20 R_e to 60 R_e, a decrease from about 16 to 8 γ (16 to 8 nT) is to be expected. At about 1000 R_e, the field intensity is generally between 4 and 16 γ (4 and 16 nT). The direction of the field in the magnetotail is generally close to the plane of the ecliptic and at a solar coordinate angle Φ_{SE} (appendix A) between

270° and 360°. Field lines from the Earth's southern hemisphere are predominantly directed in an antisolar direction and separated by the neutral sheet from field lines from the northern hemisphere which are predominantly solar directed.

3.4.6 Neutral Sheet

The neutral sheet is a region within the magnetotail where abrupt reversal of the magnetic field from the solar to the antisolar direction occurs and in which magnetic intensity decreases to 4 γ (4 nT) or less. The magnetic field intensity in the neutral sheet is about 1 to 4 γ (1 to 4 nT) on the dawn meridian side and less than 1 γ (1 nT) on the side near the noon-midnight meridian plane. This sheet extends from about 10 ± 3 R_e to 1000 R_e or to the limit of the magnetotail. Its thickness varies from about 500 km to about 5000 km.

3.5 Interplanetary

An analytical model is not available for use in evaluating the interplanetary magnetic field. This field can be described as having a spiral type geometry divided into sections of constant polarity. The interplanetary field has a range of 2 to 40 γ (2 to 40 nT) with an average magnitude of 6 γ (6 nT) near Earth's orbit.

3.6 Planets and Their Natural Satellites

Analytical models are not available for any of the planets (other than Earth) or their natural satellites. Space flight data has established bounds for the magnetic fields of Venus as less than 35 γ (35 nT), Mars as less than 100 γ (100 nT) at the surface, and the Moon as less than 8 γ (8 nT) at the surface. The surface magnetic field at the equator of Jupiter is estimated to be about 5 gauss (.0005T). Jupiter's dipole moment is expected to be 10^4 times that of the Earth's (ref. 16). In the vicinity of Jupiter's shock front, the interplanetary field is estimated to be about 0.7 γ (0.7 nT).

REFERENCES

1. Anon.: Spacecraft Magnetic Torques. NASA SP-8018. Dec. 1968.

2. Parsons, C.L.; and Harris, C.A.: Component Magnetic Test Facility Operations and Test Procedure Manual. NASA TM X-55495, 1965.

3. Bastow, J.G., compiler: Proceedings of the Magnetics Workshop, March 30-April 1, 1965. Jet Propulsion Lab. Tech. Memo. no. 33-216, Sept. 1965.

4. Ness. N.F.: From "Orbis Virtutis" to Geomagnetosphere. MIT Tech. Review, Feb. 1968, pp. 35-40.

5. Cahill, J.J., Jr.: The Magnetosphere. Sci. American, vol. 212, no. 3, March 1965, pp. 58-68.

6. Kern, J.W.; and Vestine, E.H.: Magnetic Fields of the Earth and Planets. Rand Corp. (Santa Monica), Memorandum RM-3523-NASA, March 1963.

7. Anon.: Total Intensity of the Earth's Magnetic Force for the Year 1965. U.S. Naval Oceanographic Office, Chart no. 1703, 3rd ed., Jan. 1966.

8. Anon.: Catalog of Nautical Charts and Publications, Part I. U.S. Naval Oceanographic Office, H.O. Pub. no. 1-N, May 1968.

9. Chernosky, E.J.; Fougere, P.F.; and Hutchinson, R.O.: The Geomagnetic Field. Handbook of Geophysics and Space Environments (S.L. Valley, ed.), AF Cambridge Res. Center, 1965, pp. 11-1 - 11-61.

10. Matsushita, S.; and Campbell, W.H., eds.: Physics of Geomagnetic Phenomena. Vol. I. Academic Press, 1967.

11. Matsushita, S.; and Campbell, W.H., eds.: Physics of Geomagnetic Phenomena. Vol. II. Academic Press, 1967.

12. Mead, D.: Deformation of the Geomagnetic Field by the Solar Wind. J. Geophys. Res., vol. 69, no. 7, April 1964, pp. 1181-1195.

13. Cummings, W.D.; and Coleman, P.J., Jr.: Magnetic Fields in the Magnetopause and Vicinity at Synchronous Altitude. J. of Geophys. Res, Space Physics. vol. 73, no. 17, Sept. 1, 1968.

14. Anderson, K.A.; and Ness, N.F.: Correlation of Magnetic Fields and Energetic Electrons on the IMP-I Satellite. J. Geophys. Res., vol. 71, no. 15, Aug. 1966, pp. 3705-3727.

15. Jenisch, W., Jr.; and Parkinson, J.B.: Space Environment Criteria, Final Report. Aerojet Corp. (Azusa, Calif.), Report no. 3147, Jan. 1966.

16. Smith, E.J.: Planetary Magnetic Field Experiments. Presented at Advanced Space Experiments Meeting, Am. Astronaut. Soc., (Ann Arbor, Mich.), Sept. 1968.

17. Maguire, J.J.; and Carovillano, R.L.: Effect of the Interplanetary Field on the Energy of Geomagnetic Disturbances. J. Geophys. Res., Sp. Phys., vol. 73, no. 11, June 1968, pp. 3395-3405.

18. Greenstadt, E.W.; Green, I.M.; Inouye, G.T.; Hundhausen, A.J.; Bame, S.J.; and Strong, I.B.: Correlated Magnetic Field and Plasma Observations of the Earth's Bow Shock. J. Geophys. Res., Sp. Phys., Vol. 73, no. 1, Jan. 1968, pp. 51-60.

19. Heppner, J.P.; Sugiura, M.; Skillman, T.L.; Ledley, B.G.; and Campbell, M.: OGO-A Magnetic Field Observations. J. Geophys. Res., vol. 72, no. 21, Nov. 1967, pp. 5417-5471.

20. Lazarus, A.J.; Siscoe, G.L.; and Ness, N.F.: Plasma and Magnetic Field Observations During the Magnetosphere Passage of Pioneer 7. J. Geophys. Res., Sp. Phys., vol. 73, no. 7, April 1968, pp. 2399-2409.

21. Ness, N.F.; Scearce, C.S.; and Cantarano, S.C.: Probable Observations of the Geomagnetic Tail at 10^3 Earth Radii by Pioneer 7. J. Geophys. Res., vol. 72, no. 15, Aug. 1967, pp. 3769-3776.

22. Ness, N.F.: The Geomagnetic Tail. NASA TM X-63330, 1968.

23. Speiser, T.W.; and Ness, N.F.:The Neutral Sheet in the Geomagnetic Tail: Its Motion, Equivalent Currents, and Field Line Connection Through It. J. Geophys. Res., vol. 72, no. 1, Jan. 1967, pp. 131-141.

24. Hoffman, R.A.; and Cahill, L.J., Jr.: Ring Current Particle Distributions Derived from Ring Current Magnetic Field Measurements. NASA TM X-63147, 1968.

25 Cain, J.C.; Hendricks, S.J.; Langel, R.A.; and Hudson, W.V.: A Proposed Model for the International Geomagnetic Reference Field - 1965. Journal of Geomagnetism and Geoelectricity, vol. 19, no. 4, 1967.

26. Luke, R.K.C.: Descriptions of the Geomagnetic Field. Tech. Report TR-1001 (2307)-5 (AF Rept. SSD-TR-67-32), Electronics Div. Control Systems Dept., Aerospace Corp. (El Segundo), Jan. 1967.

27. Heppner, J.P.: Recent Measurement of the Magnetic Field in the Outer Magnetosphere and Boundary Regions. NASA TM X-55407, 1965.

28. Mustel', E.R.: The Solar Wind and Interplanetary Magnetic Fields. Res. Trans. T-R-678, AF Cambridge Res. Labs. (Bedford, Mass.), Jan. 1968. (Trans. from Priroda, No. 7, 1967, pp. 13-23).

29. Fan, C.Y.; Pick, M.; Pyle, R.; Simpson, J.A.; and Smith, D.R.: Protons Associated with Centers of Solar Activity and Their Propagation in Interplanetary Magnetic Field Regions Corotating with the Sun. J. Geophys. Res., Sp. Phys., vol. 73, no. 5, March 1968, pp. 1555-1582.

30. Ness, N.F.: Direct Measurements of Interplanetary Magnetic Field and Plasma. NASA TM X-55830, 1967.

31. Shatten, K.H.; Wilcox, J.M.; and Ness, N.F.: A Model of Interplanetary and Coronal Magnetic Field. J. Solar Physics, vol. 6, 1969, pp. 442-455.

32. Bumba, V.: and Howard R.: Solar Magnetic Fields. Science, vol. 149, no. 3690, Sept. 1965, pp. 1331-1337.

33. Gledhill, J.A.: The Structure of Jupiter's Magnetosphere and the Effect of Io on its Decametric Radio Emission. NASA TM X-55980, 1967.

34 Bridge, H.S.; Lazarus, A.J.; Snyder, C.W.; Smith, E.J.; Davis, L., Jr.; Coleman, P.J., Jr.; and Jones, D.E.: Mariner V: Plasma and Magnetic Fields Observed Near Venus. Science, vol. 158, Dec. 1967, pp. 1669-1673.

35. Smith, E.J.: A Review of Lunar and Planetary Magnetic Field Measurements Using Space Probes. Jet Propulsion Lab., Tech. Report 32-1059, 1965. (Also available in Magnetism and the Cosmos. Oliver & Boyd Ltd., Edinburgh.)

36. Newell, H.E.: NASA's Space Science and Applications Program. Statement presented to Comm. on Aeronautical & Space Sciences, U.S. Senate, April 20, 1967, hearing no. 1296, pp. 365-395.

37. Warwick, J.J.: Mechanisms of Decameter Radiation. Report AFCRL-64-774, Air Force Cambridge Res. Labs, Sept. 1964.

38. Smith, A.G.; and Carr, T.D.: Radio Exploration of the Planetary System. Van Nostrand Co., 1964, pp. 107-108.

39. Moroz, V.I.: Physics of Planets. NASA TT F-515, April 1968, pp. 371-372.

40. Ness, N.F.; Behannon, K.W.; Scearce, C.S.; and Cantarano, S.C.: Early Results from the Magnetic Field Experiment on Lunar Explorer 35. NASA TM X-55847, 1967.

41. Ness, N.F.; Behannon, K.W.; Taylor, H.E.; and Whang, Y.C.: Perturbations of the Interplanetary Magnetic Field by the Lunar Wake. J. Geophys. Res., Sp. Phys., vol. 73, no. 11, June 1, 1968, pp. 3421-3440.

42. Frank, L.A.: Observations of Magnetospheric Boundary Phenomena. Radiation Trapped in the Earth's Magnetic Field (B.M. McCormac, ed.), Gordon & Breach, Inc., 1966, pp. 422-446.

43. Goldstein, K.S.; and Gray, G.R.: Handbook of Definitions, Terms, Formulas, Conversion Tables, and Measurement Methods for Magnetic Phenomena. Apparatus Div., Texas Instruments Inc., Report 2-61042, Dec. 1963.

44. Mechtly, E.A.: The International System of Units. Physical Constants and Conversion Factors. NASA SP-7012, 1964.

45. Cain, J.C.; Daniels, W.E.; and Hendricks, S.J.: An Evaluation of the Main Geomagnetic Field, 1940-1962. J. Geophys. Res., vol. 70, no. 15, Aug. 1965, pp. 3647-3674.

46. Cain, J.C.; Hendricks, S.; Daniels, W.E.; and Jensen, D.C.: Computation of the Main Geomagnetic Field from Spherical Harmonic Expansions. NASA TM X-55105, 1964.

APPENDIX A
COORDINATE SYSTEMS AND NOMENCLATURE

Several coordinate systems are commonly used to define magnetic quantities in the context of convenient geometry for the geomagnetic field, the magnetosphere, and the solar system. The following coordinate systems are defined in this appendix: geocentric, geodetic, geomagnetic, local geomagnetic, solar ecliptic, and solar magnetospheric. Because geographic and geodetic coordinate systems are equivalent, the terms geographic and geodetic are used synonymously.

Geocentric Coordinate System

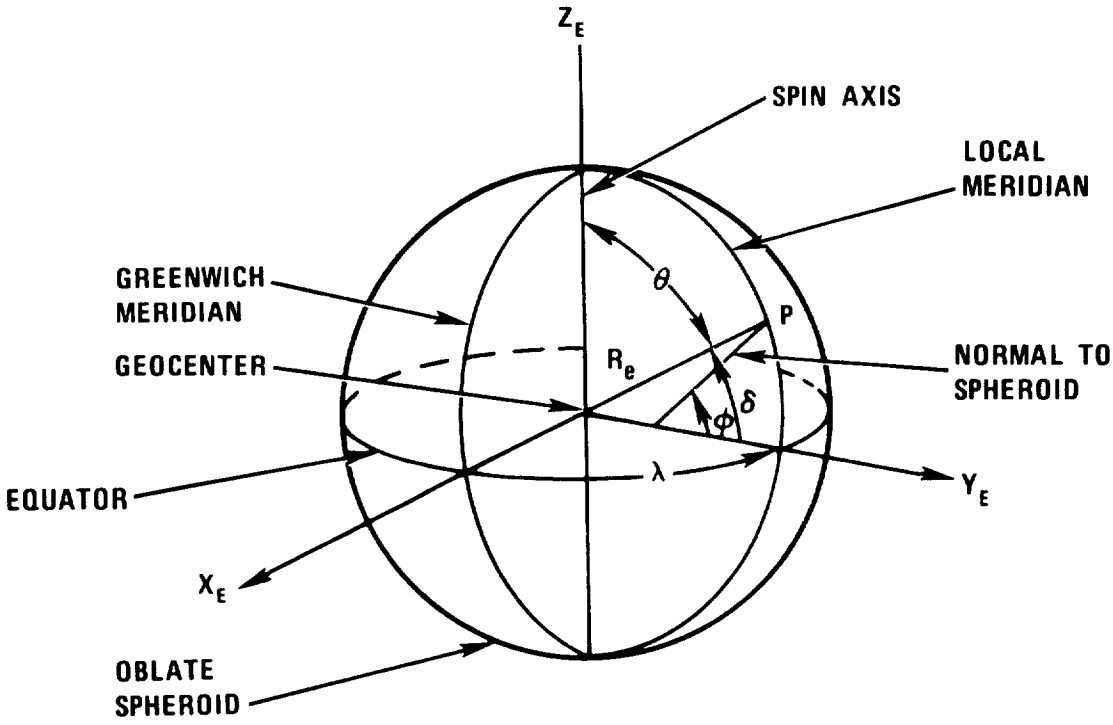

Figure A-1.–Geocentric and geodetic coordinate systems.

SYMBOLS

X_E	Positively directed along intersection of Greenwich Meridian and Equatorial planes
Z_E	Positively directed north along Earth's mean spin axis
Y_E	$Z_E \times X_E$
λ	Geocentric longitude, measured positive eastward from Greenwich meridian to local meridian

δ	Geocentric latitude, declination measured positive north (geocentric and geodetic latitude differs by 11.6 minutes maximum at 45° latitude.)
θ	Geocentric colatitude = 90° - δ
R_e	Mean Earth radius, 6371.2 km
λ	Geodetic longitude = geocentric longitude
ϕ	Geodetic latitude, measured positive north from Equatorial plane to normal to Spheroid

Geomagnetic Dipole Coordinate System

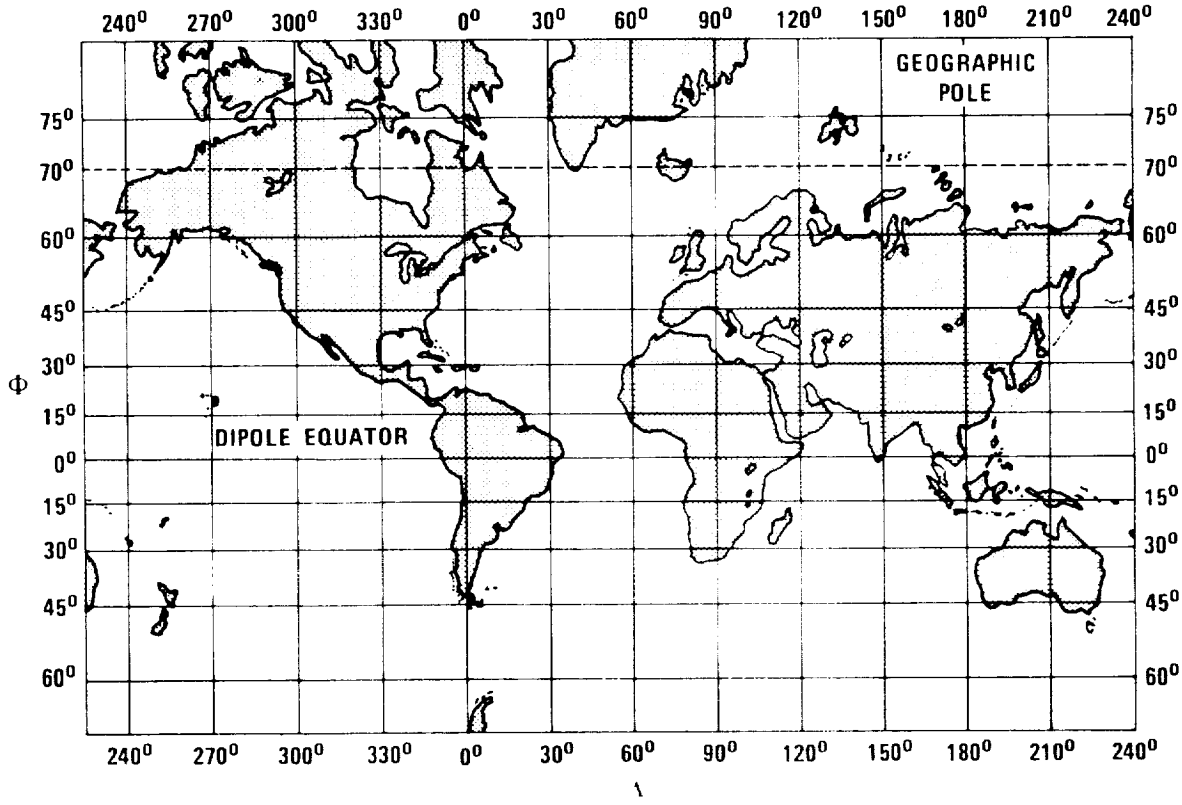

Figure A-2 – Geomagnetic dipole coordinate system (ref. 9).

SYMBOLS

Λ	Dipole eastward longitude, angular distance from great circle of spherical Earth which passes through both geographical and calculated dipole poles.
Φ	Dipole latitude, angular distance north or south of dipole equator.

DEFINITIONS

Dipole North Pole.–Defined by axis of calculated central dipole whose magnetic field is best fit to main geomagnetic field over Earth's surface and whose axis passes through geocenter. Defined to be at 78.5°N, 69.0°W in northwestern Greenland.

Dipole Equator. –Defined as great circle of spherical Earth which is normal to central dipole axis.

Dip North Pole. –Shifting point on Earth's surface where geomagnetic field lines are vertical. Location changes by a few kilometers during any day in response to transient magnetic fields. Located northwest of Hudson Bay at about 73°N, 98°W.

Geodetic to Dipole Transformation.– This is defined by the following equations (ref. 11):

$$\sin \Lambda = \frac{\cos \phi \sin (\lambda - 291°)}{\cos \Phi}$$

$$\sin \Phi = \sin \phi \cos 11.7° + \cos \phi \sin 11.7° \cos (\lambda - 291°)$$

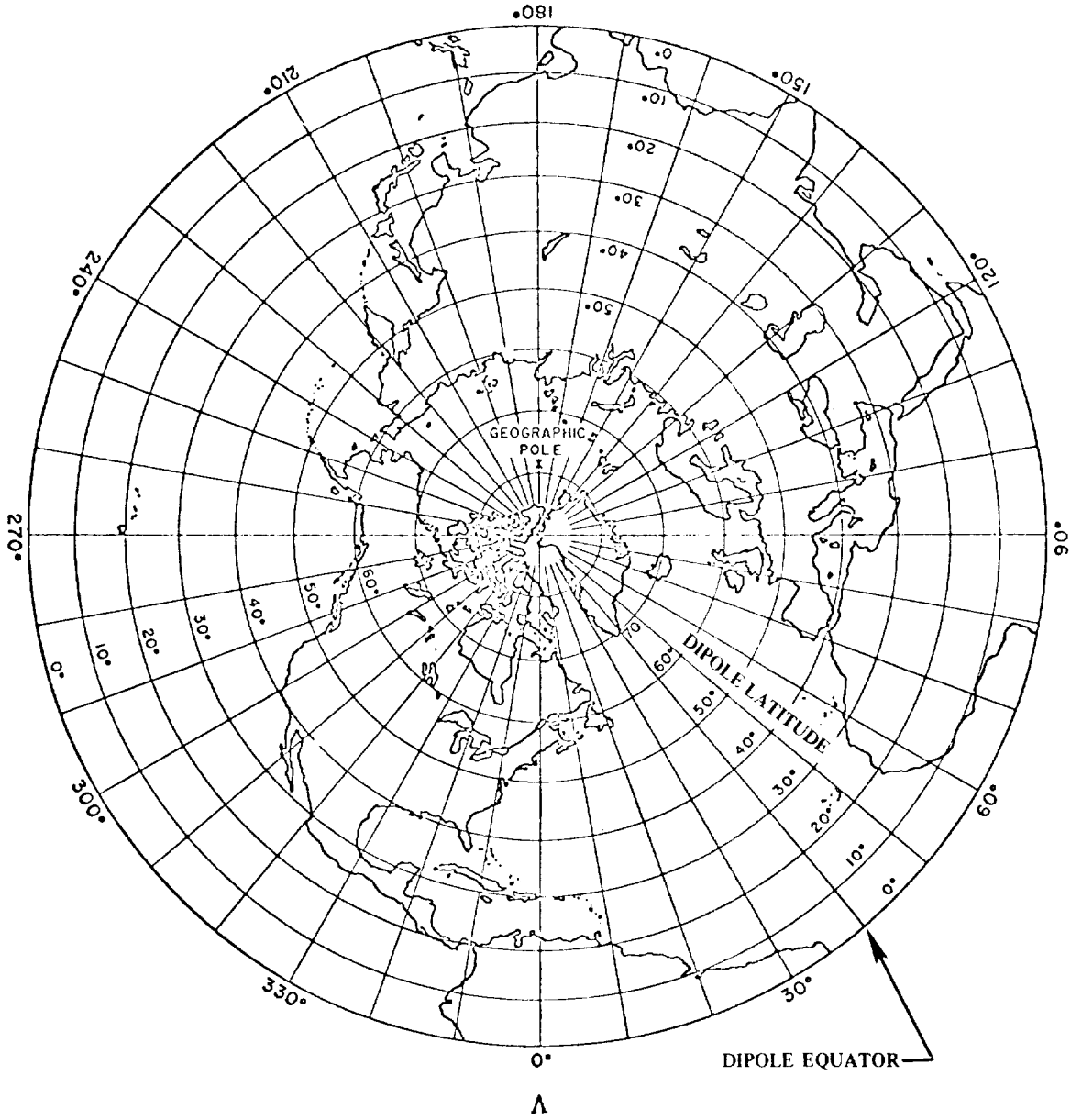

Figure A-3 – Geomagnetic dipole coordinates of Northern Hemisphere (ref. 9).

Local Geomagnetic Coordinate System

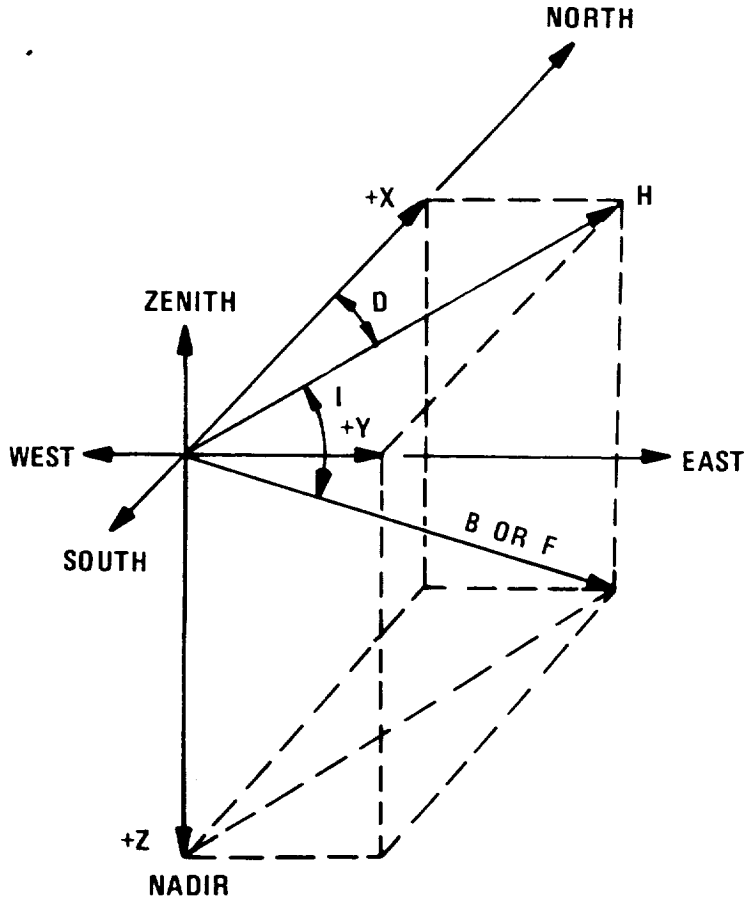

Figure A-4. Local geomagnetic coordinate system (ref. 9).

SYMBOLS

B	Total computed magnetic field intensity (total magnetic flux density - SI nomenclature)
F	Total measured field intensity
$X(B_X)$	North component of B

$Z (B_Z, V)$	Vertical component of B
$Y (B_Y)$	East component of B ($Z \times X$)
I	Inclination or dip angle
H	Horizontal field intensity (B cos I)
D	Declination angle

Solar Ecliptic Coordinate System

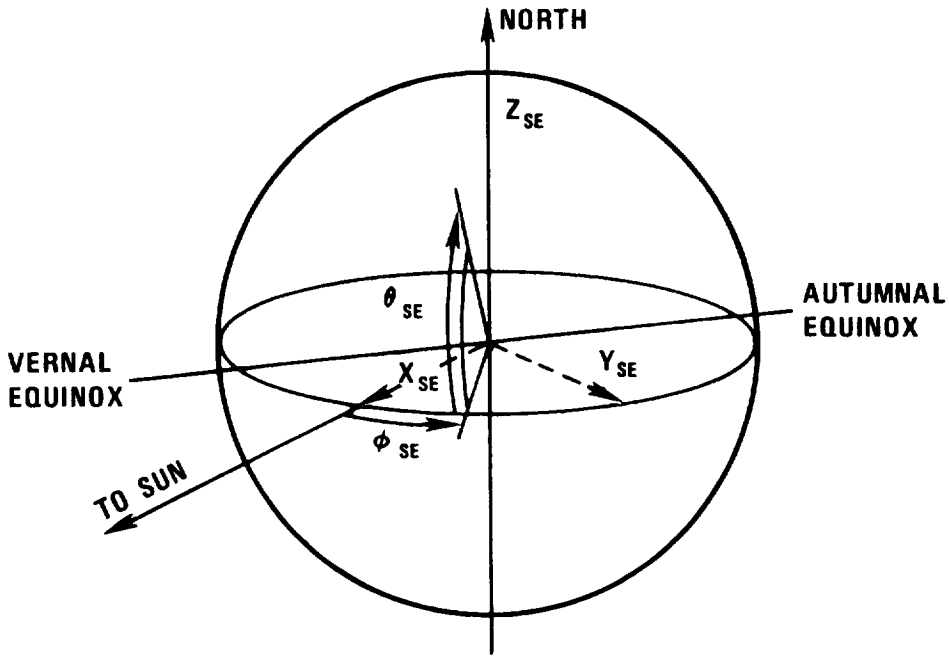

Figure A-5.—Solar ecliptic coordinate system (ref. 42).

SYMBOLS

X_{SE}	Positively directed toward Sun along Earth-Sun line
Z_{SE}	Positively directed toward north ecliptic pole
Y_{SE}	$Z_{SE} \times X_{SE}$

θ_{SE} Solar ecliptic latitude

ϕ_{SE} Solar ecliptic longitude

Solar Magnetospheric Coordinate System

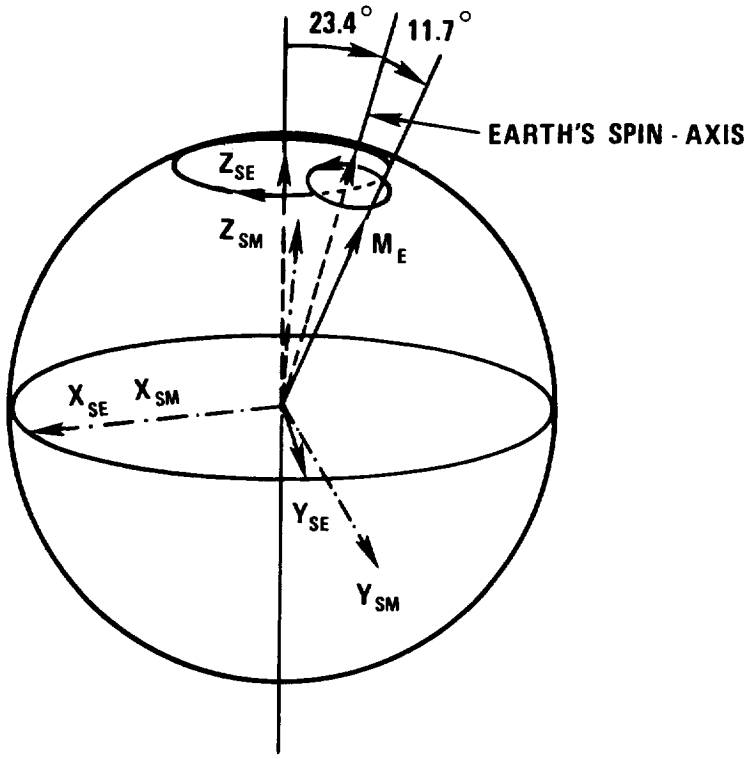

Figure A-6.–Solar magnetosphiric coordinate system (ref. 42).

SYMBOLS

M_E Positively directed northward parallel to Earth's magnetic dipole axis

S_E Positively directed northward parallel to Earth's spin axis

X_{SM} Positively directed toward Sun along Earth-Sun line (parallel to X_{SE})

Z_{SM} $X_{SM} \times Y_{SM}$

Y_{SM} Parallel to $M_E \times X_{SM}$

APPENDIX B
DIMENSIONS, UNITS, AND CONVERSION FACTORS

Several systems of units have been commonly used to describe the characteristics of magnetic fields. The system of electrostatic units (esu) uses Coulomb's law; and the system of electromagnetic units (emu) uses the law of attraction between currents. The Gaussian system expresses magnetic quantities in emu and electric quantities in esu. In the Gaussian system, the magnetic flux density (**B**) and the magnetic field intensity (**H**) are used interchangeably. This interchangeability is based on the fact that $\mathbf{B} = \mu \mathbf{H}$, where the permeability μ, is unity for a non-magnetic medium, in which case $\mathbf{B} = \mathbf{H}$. The unit for **B** and **H** was the gauss until 1932. After 1932, **H** was expressed in oersted. Another unit used for **B** and **H** is gamma (γ) which was first introduced in studies of geomagnetism. When μ is unity, gamma is equal to 10^{-5} gauss and is validly used for both field intensity and flux density (ref. 43). In 1960, the Eleventh General Conference on Weights and Measures adopted the metric system of units (meter, kilogram, second, ampere, Kelvin degree, and candela) as the international standard. This system was named the International System of Units (SI). In SI units, the tesla (T) is the unit of magnetic flux density and the ampere per meter (A/m) is the unit of magnetic field strength (ref. 44).

Dimensions and units used in this monograph are in terms of both the Gaussian system and the International System. Relations between the SI metric system of units and emu and esu systems are given below for the following quantities: magnetic field intensity, magnetic flux, magnetic field strength, magnetic dipole moment, and current (ref. 44).

TABLE B-1 Magnetic Field Intensity (Magnetic Flux Density in SI Nomenclature)*

System of Units	one \ equals	T	Γ	γ
SI	webers / meter^2 (Wb / m^2) or tesla (T)	1	10^4	10^9
emu	gauss (Γ)	10^{-4}	1	10^5
**	gamma (γ)	10^{-9}***	10^{-5}	1

* Vector components of field intensity are defined in figure A - 4 of appendix A.
** Not part of a system.
*** 1 nanotesla (nT)

TABLE B-2 Magnetic Flux (Φ_B)

System of Units	one \ equals	Wb	line
SI	weber (Wb)	1	10^8
emu	maxwell (line)	10^{-8}	1

TABLE B-3 Magnetic Field Strength (H)

System of Units	one \ equals	A/m	Oe	γ
SI	ampere / meter (A / m)	1	$4\pi \times 10^{-3}$	$4\pi \times 10^2$
emu	oersted (Oe)	$10^3 / 4\pi$	1	10^5
*	gamma (γ)	$10^{-2} / 4\pi$	10^{-5}	1

* Not part of a system

TABLE B-4 Magnetic Dipole Moment ($\vec{\mu}$)

System of Units	one \ equals	Loop: $A\text{-}m^2$	Dipole: Wb-m	Loop: pole-cm	Dipole: pole-cm
SI	ampere-meter^2 ($A\text{-}m^2$)	1	$4\pi \times 10^{-7}$	10^3	10^3
	weber-meter (Wb-m)	$\frac{10^7}{4\pi}$	1	$\frac{10^{10}}{4\pi}$	$\frac{10^{10}}{4\pi}$
emu	pole - centimeter (pole - cm or upc)	10^{-3}	$4\pi \times 10^{-10}$	1	1

Note: In cgs units the following are often used interchangeably for magnetic moment: pole - cm; gauss - cm^3; dyne - cm / oersted; dyne - cm / gauss.

TABLE B-5 Current

System of Units	one \ equals	A	abA	statA
SI	ampere (A)	1	0.1	3×10^9
emu	abampere (abA)	10	1	3×10^{10}
esu	statampere (statA)	$\frac{1}{3} \times 10^{-9}$	$\frac{1}{3} \times 10^{-10}$	1

APPENDIX C
MODELS OF THE EARTH'S MAGNETIC ENVIRONMENT

Spherical Harmonic Expansion Model

The spherical harmonic expansion model is a series expansion in spherical coordinates of the magnetic flux density (B) which is defined as the negative gradient of the geomagnetic potential function V, where

$$V = R_e \sum_{n=1}^{\infty} \sum_{m=0}^{n} \left(\frac{R_e}{R}\right)^{n+1} \left(g_n^m \cos m\lambda + h_n^m \sin m\lambda\right) P_n^m (\cos\theta) \quad \text{(C-1)}$$

R_e = mean Earth radius (6371.2 km)

R = distance from geocenter

g_n^m and h_n^m = harmonic coefficients

λ = geocentric east longitude

θ = geocentric colatitude ($90° - \delta$)

δ = geocentric latitude

$P_n^m (\cos\theta)$ = Schmidt function - partially normalized spherical harmonic function of degree n and order m with $m \leq n$.

The harmonic coefficients g_n^m and h_n^m are determined by analyzing measurements of the geomagnetic field components made at a large number of points on the Earth's surface. Table C-1 (ref. 25) gives a set of 120 of these coefficients with their first and second derivatives.

The Schmidt functions are defined as:

$$P_n^m(\cos\theta) = \begin{cases} P_{n,m}(\cos\theta) & \text{for } m = 0 \\ \left[\frac{2(n-m)!}{(n+m)!}\right]^{1/2} \left[P_{n,m}(\cos\theta)\right] & \text{for } m \neq 0 \end{cases} \quad \text{(C-2)}$$

The associated Legendre function, $P_{n,m}(\cos\theta)$, is given by

$$P_{n,m}(\cos\theta) = \frac{(2n)!}{2^n n!\,(n-m)!} \sin^m\theta \left[(\cos\theta)^{n-m} - \frac{(n-m)(n-m-1)}{2(2n-1)}(\cos\theta)^{n-m-2}\right.$$

$$\left. + \frac{(n-m)(n-m-1)(n-m-2)(n-m-3)}{2(4)(2n-1)(2n-3)}(\cos\theta)^{n-m-4} + \ldots\right] \quad \text{(C-3)}$$

To calculate components of B at some point in space, the following relations are used:*

$$B_X = \frac{1}{R}\frac{\partial V}{\partial\theta} = \sum_{n=1}^{\infty}\sum_{m=0}^{n}\left(\frac{R_e}{R}\right)^{n+2} \frac{dP_n^m(\cos\theta)}{d\theta}\left[g_n^m \cos m\lambda + h_n^m \sin m\lambda\right] \quad \text{(C-4)}$$

$$B_Y = -\frac{1}{R\sin\theta}\frac{\partial V}{\partial\lambda} = \sum_{n=1}^{\infty}\sum_{m=0}^{\infty}\left(\frac{R_e}{R}\right)^{n+2} \frac{mP_n^m(\cos\theta)}{\sin\theta}\left[g_n^m \sin m\lambda - h_n^m \cos m\lambda\right] \quad \text{(C-5)}$$

$$B_Z = \frac{\partial V}{\partial R} = -\sum_{n=1}^{\infty}\sum_{m=0}^{n}\left(\frac{R_e}{R}\right)^{n+2} (n+1)P_n^m(\cos\theta)\left[g_n^m \cos m\lambda + h_n^m \sin m\lambda\right] \quad \text{(C-6)}$$

*Refer to appendix A for definition of geocentric coordinate system.

where:

$$\left.\begin{aligned}
\frac{dP_n^m(\cos\theta)}{d\theta} &= -\left[\frac{n}{2}(n+1)\right]^{1/2} P_n^1(\cos\theta) && \text{for } m = 0 \\
\frac{dP_n^m(\cos\theta)}{d\theta} &= \tfrac{1}{2}\left[\delta_{m-1}(n+m)(n-m+1)\right]^{1/2} P_n^{m-1}(\cos\theta) \\
&\quad - \tfrac{1}{2}\left[(n+m+1)(n-m)\right]^{1/2} P_n^{m+1}(\cos\theta) && \text{for } m \neq 0
\end{aligned}\right\} \quad \text{(C-7)}$$

and

$$\delta_{m-1} = 2 \qquad \text{for } m = 1$$

$$\delta_{m-1} = 1 \qquad \text{for } m \geq 2$$

The coordinates of a point or points in space and the number of coefficients (corrected for secular variation) needed to obtain the desired accuracy are substituted into equations C-4 through C-6. Secular variation correction is computed by adding the secular change in the coefficient over a period of time to the original coefficient. The corrected coefficient is defined as:

$$g_n^m(t) = g_n^m(\bar{t}) + (t-\bar{t})\,\dot{g}_n^m(\bar{t}) \qquad \text{(C-8)}$$

$$h_n^m(t) = h_n^m(\bar{t}) + (t-\bar{t})\,\dot{h}_n^m(\bar{t}) \qquad \text{(C-9)}$$

where $\bar{t}$ is the epoch in years for which the coefficients were derived and t is the particular time of interest (table C-1). Figure C-1 illustrates the relation between the number of coefficients (k) used in the equations and the accuracy obtained for k to 63 terms based on a set of coefficients published in 1965 (ref. 45). The decimal residual (R) is defined as the ratio of the rms of the computed values minus observed values to the observed values:

$$R = \sqrt{\sum_{i=1}^{I}\left[\frac{F_i - F_i^o}{I-1}\right]^2 \Big/ \sum_{i=1}^{I}\left[\frac{F_i^o}{I-1}\right]^2} \qquad \text{(C-10)}$$

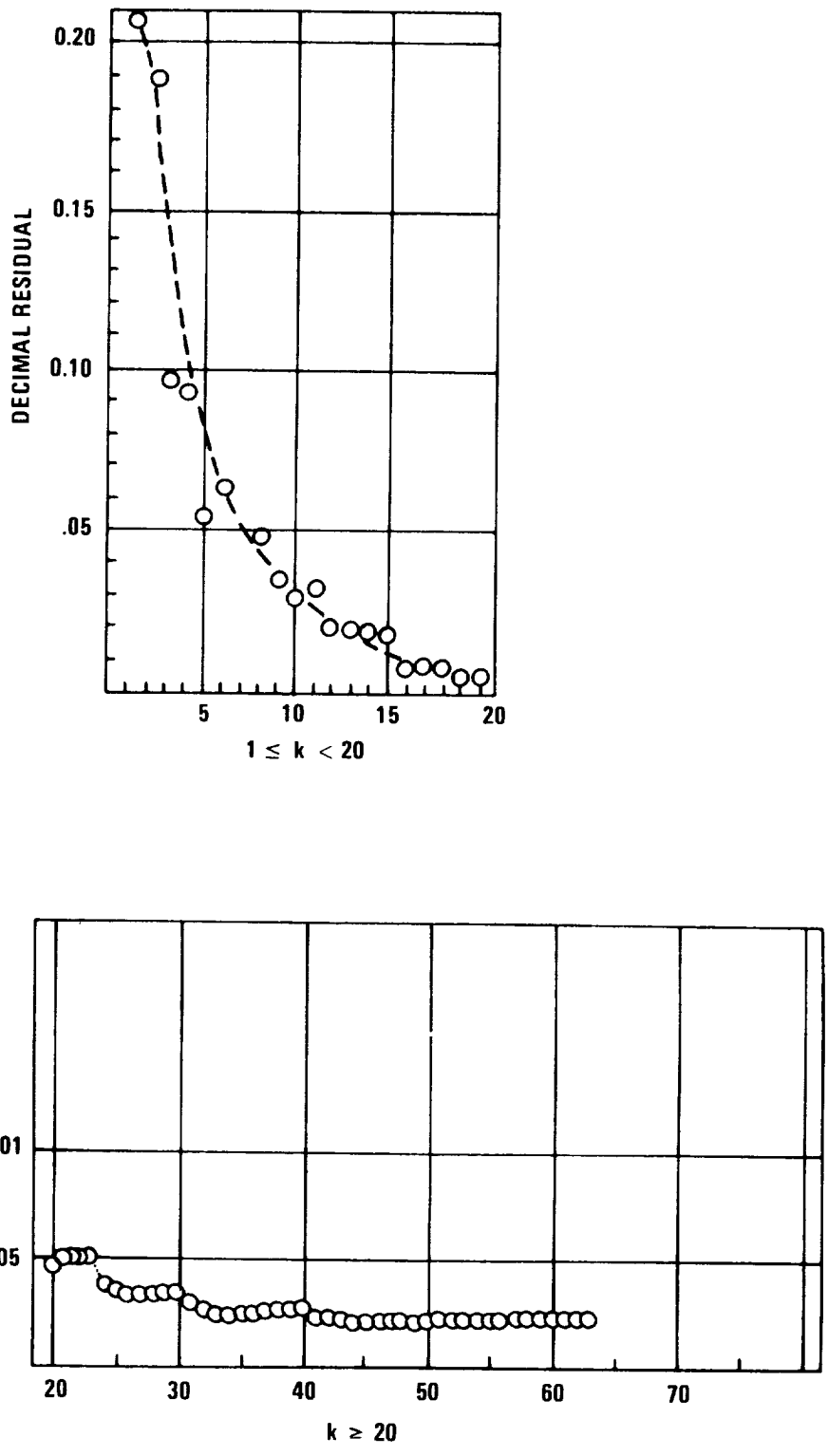

Figure C-1. -Spherical harmonic expansion accuracy as function of number of coefficients used.

Table C-1 Spherical Harmonic Coefficients (Epoch 1965.0) (ref. 25)

n	m	g (Y)	h	$\dot{g}$ (Y/yr)	$\dot{h}$	$\ddot{g}$ (Y/yr^2)	$\ddot{h}$
1	0	-30401.2	000.0	14.03	0.00	-0.062	0.000
1	1	-2163.8	5778.2	8.76	-3.71	0.114	-0.043
2	0	-1540.1	0000.0	-23.29	0.00	-0.154	0.000
2	1	2997.9	-1932.0	-0.09	-14.31	-0.018	0.054
2	2	1590.3	202.9	-4.56	-16.62	-0.253	-0.016
3	0	1307.1	000.0	-8.93	00.00	-0.123	0.000
3	1	-1988.9	-425.4	-10.62	5.20	-0.027	0.095
3	2	1276.8	227.8	2.31	2.53	0.028	-0.007
3	3	881.2	-133.8	-5.89	-6.98	-0.183	0.079
4	0	949.3	000.0	1.45	0.00	0.001	0.000
4	1	803.5	160.3	0.90	-2.19	-0.044	0.004
4	2	502.9	-274.3	-1.75	-0.14	0.017	0.056
4	3	-397.7	2.3	0.66	1.88	0.007	-0.035
4	4	266.5	-246.6	-3.01	-6.52	-0.097	-0.047
5	0	-233.5	000.0	1.61	0.00	0.045	0.000
5	1	355.7	5.1	0.60	2.24	0.001	-0.046
5	2	228.4	117.8	3.34	1.59	0.075	0.007
5	3	-28.8	-114.8	-0.04	-2.61	0.008	-0.007
5	4	-157.9	-108.9	-0.60	0.50	0.015	0.001
5	5	-62.2	82.4	1.76	-0.12	0.056	-0.024
6	0	49.2	00.0	-0.42	0.00	-0.006	0.000
6	1	57.5	-12.1	3.82	0.05	0.015	0.020
6	2	-0.8	104.4	0.82	0.09	0.010	-0.011
6	3	-238.3	56.6	2.35	2.55	0.050	0.015
6	4	-1.5	-23.4	0.83	-1.19	-0.011	-0.029
6	5	-2.0	-14.8	0.01	0.33	0.026	0.029
6	6	-108.4	-13.3	0.23	0.84	0.023	-0.010
7	0	72.2	00.0	-0.57	0.00	-0.014	0.000
7	1	-53.7	-53.7	-0.34	-0.96	-0.006	-0.014
7	2	7.9	27.4	-1.44	0.01	-0.034	0.016
7	3	15.6	-8.1	-0.90	0.43	-0.004	0.014
7	4	-24.3	7.0	0.03	0.75	-0.006	0.005
7	5	-3.6	24.3	-0.60	-0.33	-0.027	-0.008
7	6	15.5	-22.5	-0.17	0.49	-0.001	0.016
7	7	3.6	-21.4	-0.64	0.90	-0.004	0.011
8	0	8.5	00.0	0.35	0.00	0.006	0.000
8	1	6.5	5.4	0.50	-0.50	0.008	-0.015
8	2	-9.3	-11.7	1.70	-0.21	0.039	-0.012
8	3	-9.6	4.2	-0.11	0.03	-0.008	0.005
8	4	-6.1	-15.3	0.34	-0.79	0.015	-0.011
8	5	5.5	4.6	-0.07	0.05	-0.002	-0.000
8	6	-8.1	21.9	0.43	0.10	0.005	-0.003
8	7	13.0	-0.7	-0.15	-0.36	-0.008	-0.009
8	8	7.4	-17.1	-0.42	-0.43	-0.007	-0.003
9	0	10.4	00.0	-0.10	0.00	-0.005	0.000
9	1	5.8	-22.4	-0.13	0.66	-0.001	0.022
9	2	7.5	13.8	-1.20	0.54	-0.027	0.007
9	3	-15.1	6.3	0.08	0.03	0.005	-0.002
9	4	12.1	-3.0	-0.08	0.35	-0.007	0.009
9	5	4.7	-1.9	-0.39	-0.03	-0.006	0.006
9	6	0.2	9.0	-0.36	-0.01	-0.009	-0.001
9	7	1.6	11.5	0.47	0.45	0.006	0.009
9	8	0.9	0.1	0.37	-0.05	0.005	-0.004
9	9	0.2	-1.5	-0.48	0.75	-0.009	0.019
10	0	-2.9	0.0	-0.01	0.00	-0.003	0.000
10	1	-0.9	-0.1	-0.13	-0.61	-0.003	-0.012
10	2	-2.2	4.5	0.88	-0.64	0.020	-0.014
10	3	0.8	-1.0	-0.18	0.02	-0.008	0.001
10	4	-2.8	2.6	0.17	0.05	0.007	0.001
10	5	6.4	-4.4	-0.02	-0.63	0.001	-0.011
10	6	4.7	-1.3	0.05	-0.07	0.001	-0.001
10	7	-0.2	-3.6	0.17	0.07	0.001	0.001
10	8	1.8	4.0	0.16	-0.03	0.005	-0.001
10	9	2.0	1.0	0.31	-0.02	0.004	0.001
10	10	1.1	-2.0	-0.23	-0.45	-0.002	-0.006

where

I = total number of observations

F_i = scalar field computed at each data point using indicated number of coefficients

F_i^o = respective observed value of scalar field intensity.

An alternative formulation of this model employs Gauss normalized (Gauss-LaPlace) functions, $P^{n,m}(\theta)$, rather than the Schmidt functions, $P_n^m(\theta)$. In this case, the magnetic flux density is equated to the positive gradient of the geomagnetic potential function ($B = +\nabla V$) (ref. 43).

Computer programs which provide numerical solutions of the field equations C-4 through C-6 are available at NASA Centers as well as most of the major aerospace contractors. Generally, these programs allow for variation in the number of coefficients used and thus are applicable when limitations in the storage capacity of a particular computer do not permit utilization of all the coefficients.

Reference 43 presents a set of programs which will evaluate the geomagnetic field components using any available set of coefficients at any point in normal geodetic coordinates (latitude, longitude, altitude). These programs accommodate either Gauss normalized or Schmidt functions.

Quadrupole Model

The quadrupole model uses the first eight terms of the spherical harmonic expansion to obtain an approximation of the geomagnetic field. The geomagnetic potential is approximated by:

$$V = R_e \left(\frac{R_e}{R}\right)^2 \left[g_1^0 \; P_1^0 \; (\cos\theta) + (g_1^1 \cos\lambda + h_1^1 \sin\lambda) \; P_1^1 \; (\cos\theta)\right]$$

$$+ R_e \left(\frac{R_e}{R}\right)^3 \left[g_2^0 \; P_2^0 \; (\cos\theta) + (g_2^1 \cos\lambda + h_2^1 \sin\lambda) \; P_2^1 \; (\cos\theta)\right.$$

$$\left. + (g_2^2 \cos 2\lambda + h_2^2 \sin 2\lambda) \; P_2^2 \; (\cos\theta)\right] \qquad \text{(C-11)}$$

To calculate the components of **B** at some point in space, the following are used:*

$$B_X = \frac{1}{R}\frac{\partial V}{\partial \theta} = \left(\frac{R_e}{R}\right)^3 \left[-g_1^0 \sin\theta + \cos\theta \left(g_1^1 \cos\lambda + h_1^1 \sin\lambda\right)\right]$$

$$+\left(\frac{R_e}{R}\right)^4 \left[-3\, g_2^0 \sin\theta \cos\theta + \sqrt{3}\left(2\cos^2\theta - 1\right)\left(g_2^1 \cos\lambda + h_2^1 \sin\lambda\right)\right.$$

$$\left.+\left(\sqrt{3}\sin\theta\cos\theta\right)\left(g_2^2 \cos 2\lambda + h_2^2 \sin 2\lambda\right)\right] \qquad \text{(C-12)}$$

$$B_Y = -\frac{1}{R\sin\theta}\frac{\partial V}{\partial \lambda} = \left(\frac{R_e}{R}\right)^3 \left[g_1^1 \sin\lambda - h_1^1 \cos\lambda\right]$$

$$+\left(\frac{R_e}{R}\right)^4 \left[\sqrt{3}\cos\theta \left(g_2^1 \sin\lambda - h_2^1 \cos\lambda\right)\right.$$

$$\left.+\sin\theta \left(g_2^2 \sin 2\lambda - h_2^2 \cos 2\lambda\right)\right] \qquad \text{(C-13)}$$

$$B_Z = \frac{\partial V}{\partial R} = -\left(\frac{R_e}{R}\right)^3 \left[2\, g_1^0 \cos\theta + 2\sin\theta \left(g_1^1 \cos\lambda + h_1^1 \sin\lambda\right)\right]$$

$$-3\left(\frac{R_e}{R}\right)^4 \left[\left(\frac{3}{2}\cos^2\theta - \frac{1}{2}\right)\left(g_2^0\right) + \sqrt{3}\sin\theta\cos\theta \left(g_2^1 \cos\lambda + h_2^1 \sin\lambda\right)\right.$$

$$\left.+\left(\frac{1}{2}\sin^2\theta\right)\left(g_2^2 \cos^2\lambda + h_2^2 \sin 2\lambda\right)\right] \qquad \text{(C-14)}$$

The accuracy of the quadrupole model compared to the spherical harmonic expansion model is illustrated in figures C-2 through C-6 (ref. 26). The magnitude ratio is defined as the ratio of the **B** computed by the approximation model to the **B** computed from the spherical harmonic expansion model. The angular deviation is defined as the field angle computed by the approximation model less the field angle computed by the spherical harmonic expansion model.

*Refer to appendix A for definition of geocentric coordinate system.

Dipole Models

Spin-Axis Dipole Model

The spin-axis dipole model uses the first term of the spherical harmonic expansion to obtain an approximation of the geomagnetic field which is generally lower than the actual field. The geomagnetic potential is approximated by:

$$V = R_e \left(\frac{R_e}{R}\right)^2 g_1^0 P_1^0 (\cos\theta) \tag{C-15}$$

To calculate the components of B at some point in space, the following relations are used:*

$$B_x = \left(\frac{R_e}{R}\right)^3 g_1^0 \sin\theta \tag{C-16}$$

$$B_y = 0 \tag{C-17}$$

$$B_z = 2\left(\frac{R_e}{R}\right)^3 g_1^0 \cos\theta \tag{C-18}$$

The accuracy of the spin-axis dipole model compared to the spherical harmonic expansion model is illustrated in figures C-2 through C-4 (ref. 26).

Tilted Dipole Model

The tilted dipole model uses the first three terms of the spherical harmonic expansion to obtain an approximation of the geomagnetic field. The geomagnetic potential is approximated by:

$$V = R_e \left(\frac{R_e}{R}\right)^2 \left[g_1^0 P_1^0 (\cos\theta) + (g_1^1 \cos\lambda + h_1^1 \sin\lambda) P_1^1 (\cos\theta) \right] \tag{C-19}$$

To calculate the components of B at some point in space, the following relations are used:*

$$B_x = \left(\frac{R_e}{R}\right)^3 \left[-g_1^0 \sin\theta + g_1^1 \cos\theta \cos\lambda + h_1^1 \cos\theta \sin\lambda \right] \tag{C-20}$$

*Refer to appendix A for definition of geocentric coordinate system.

$$B_y = \left(\frac{R_e}{R}\right)^3 \left[g_1^1 \sin\lambda - h_1^1 \cos\lambda \right] \tag{C-21}$$

$$B_z = -2\left(\frac{R_e}{R}\right)^3 \left[g_1^0 \cos\theta + g_1^1 \sin\theta \cos\lambda + h_1^1 \sin\theta \sin\lambda \right] \tag{C-22}$$

The accuracy of the tilted dipole model compared to the spherical harmonic expansion model is illustrated in figures C-2, C-3, C-4, C-7, and C-8 (ref. 26).

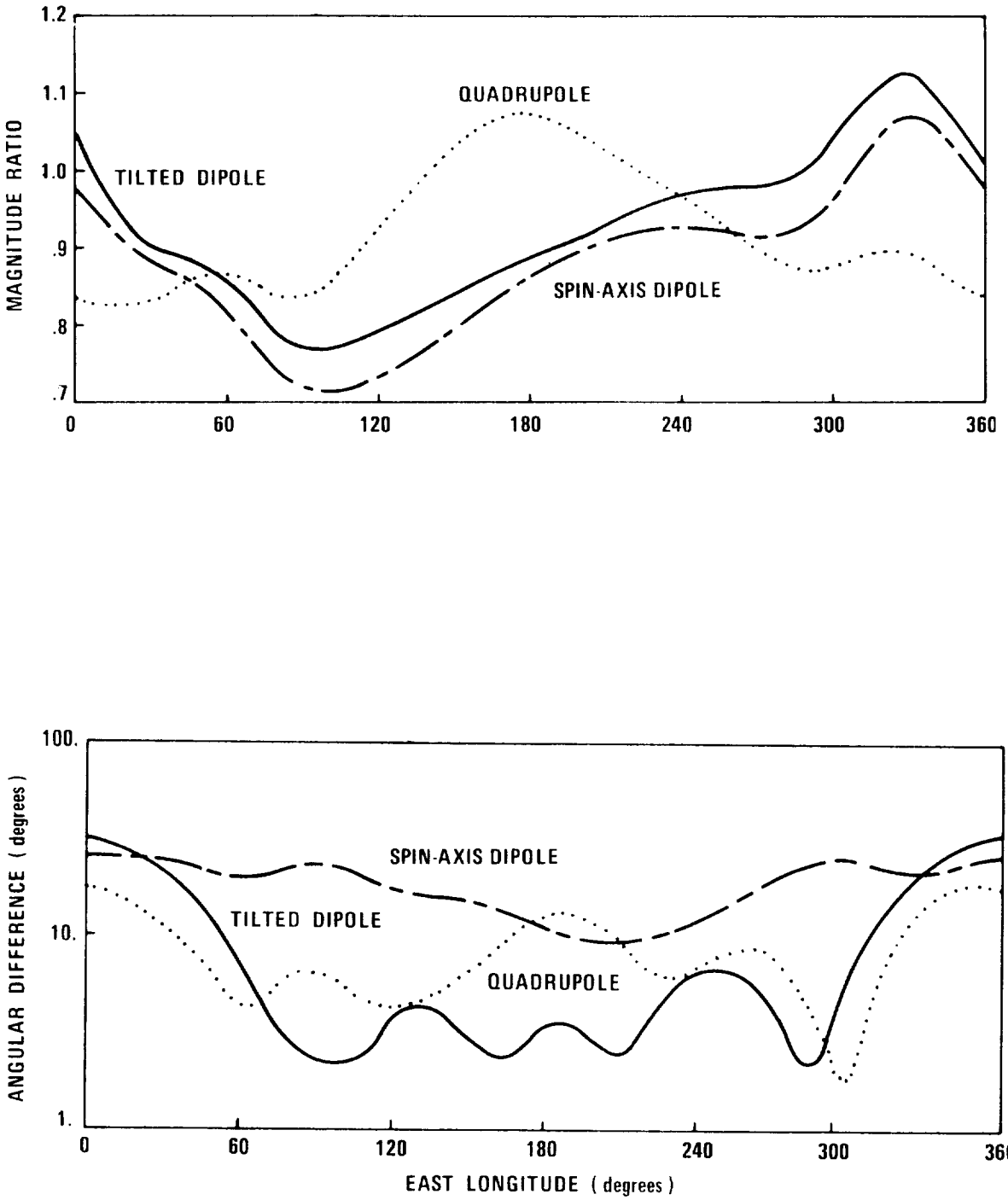

Figure C-2.–Deviation of approximation models from spherical harmonic expansion model in equatorial plane at one R_e (Earth's surface) (ref. 26).

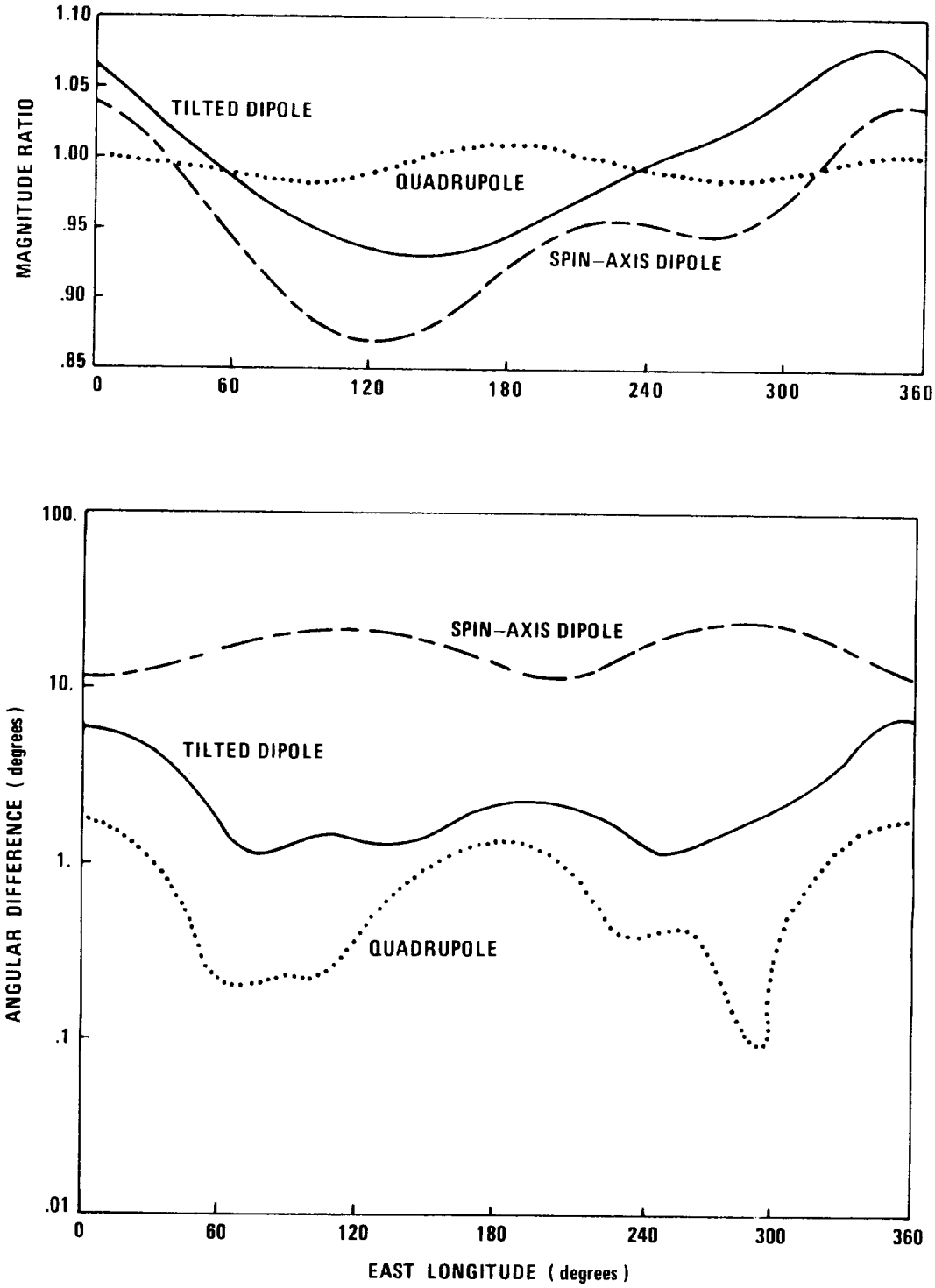

Figure C-3.–Deviation of approximation models from spherical harmonic expansion model in equatorial plane at three R_e (ref. 26).

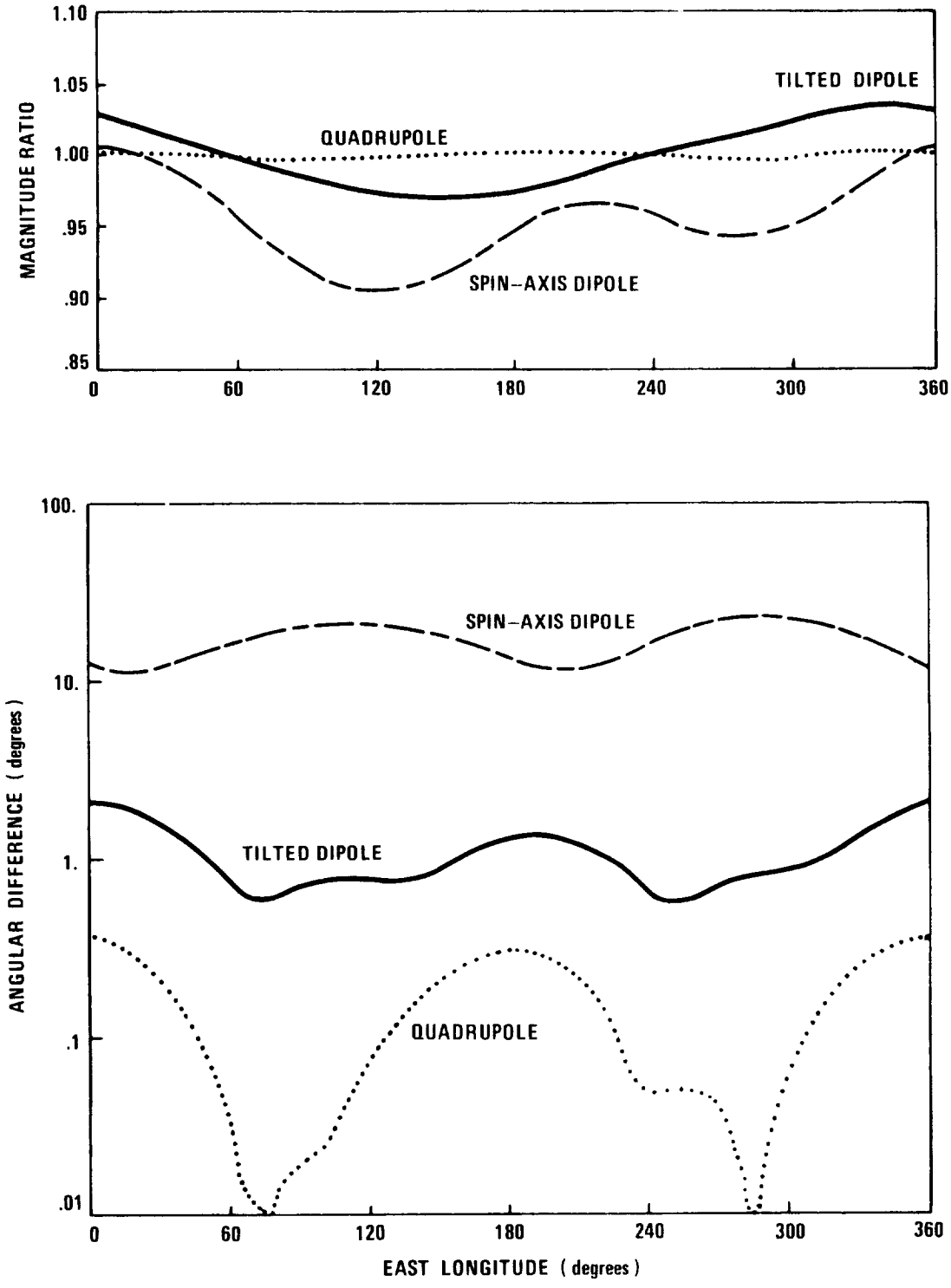

Figure C-4.–Deviation of approximation models from spherical harmonic expansion model in equatorial plane at 6.6 R_e (synchronous orbit) (ref. 26).

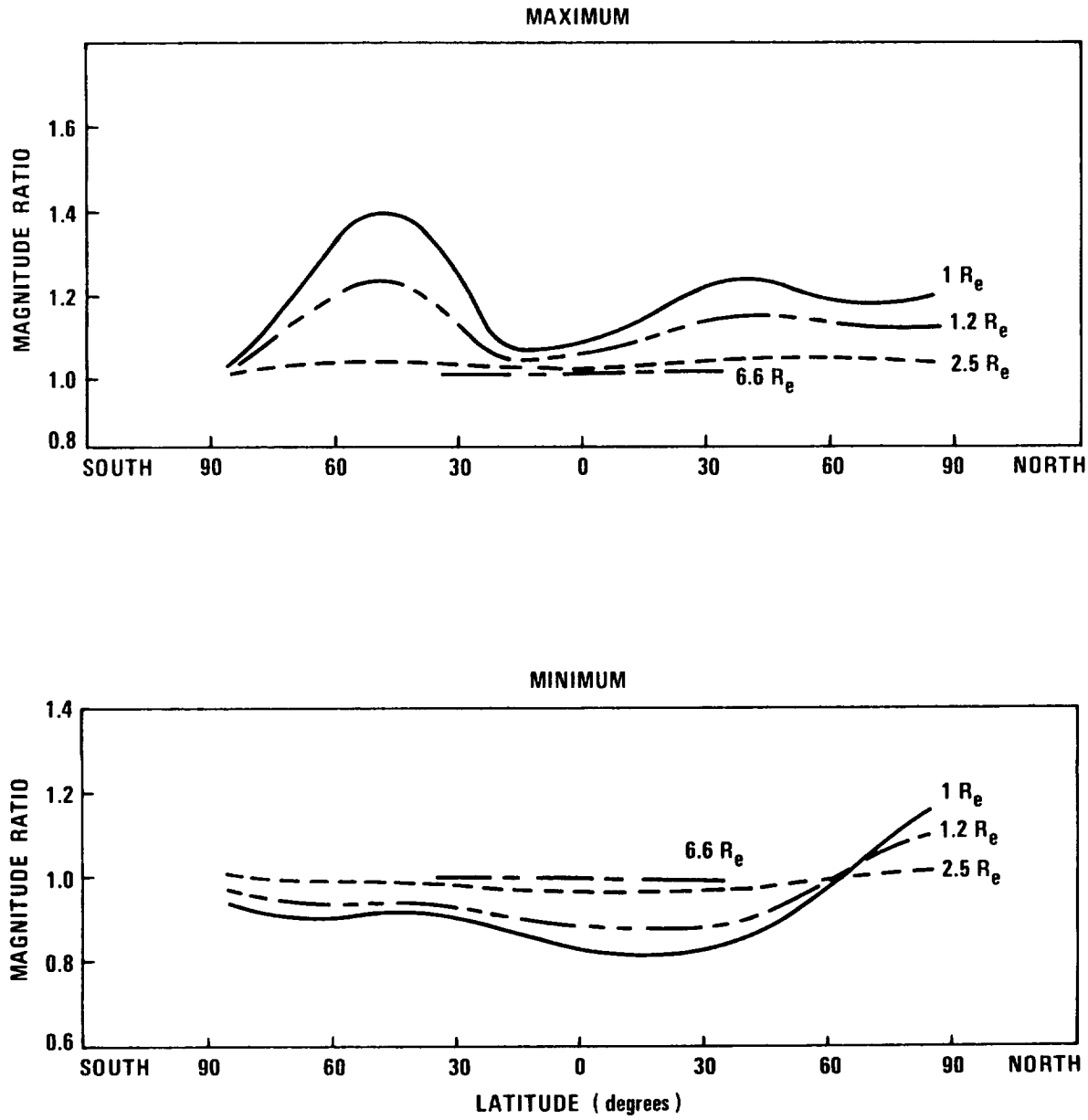

Figure C-5.–Maximum and minimum magnitude ratios of quadrupole model to the spherical harmonic expansion model at selected geocentric distances (ref. 26).

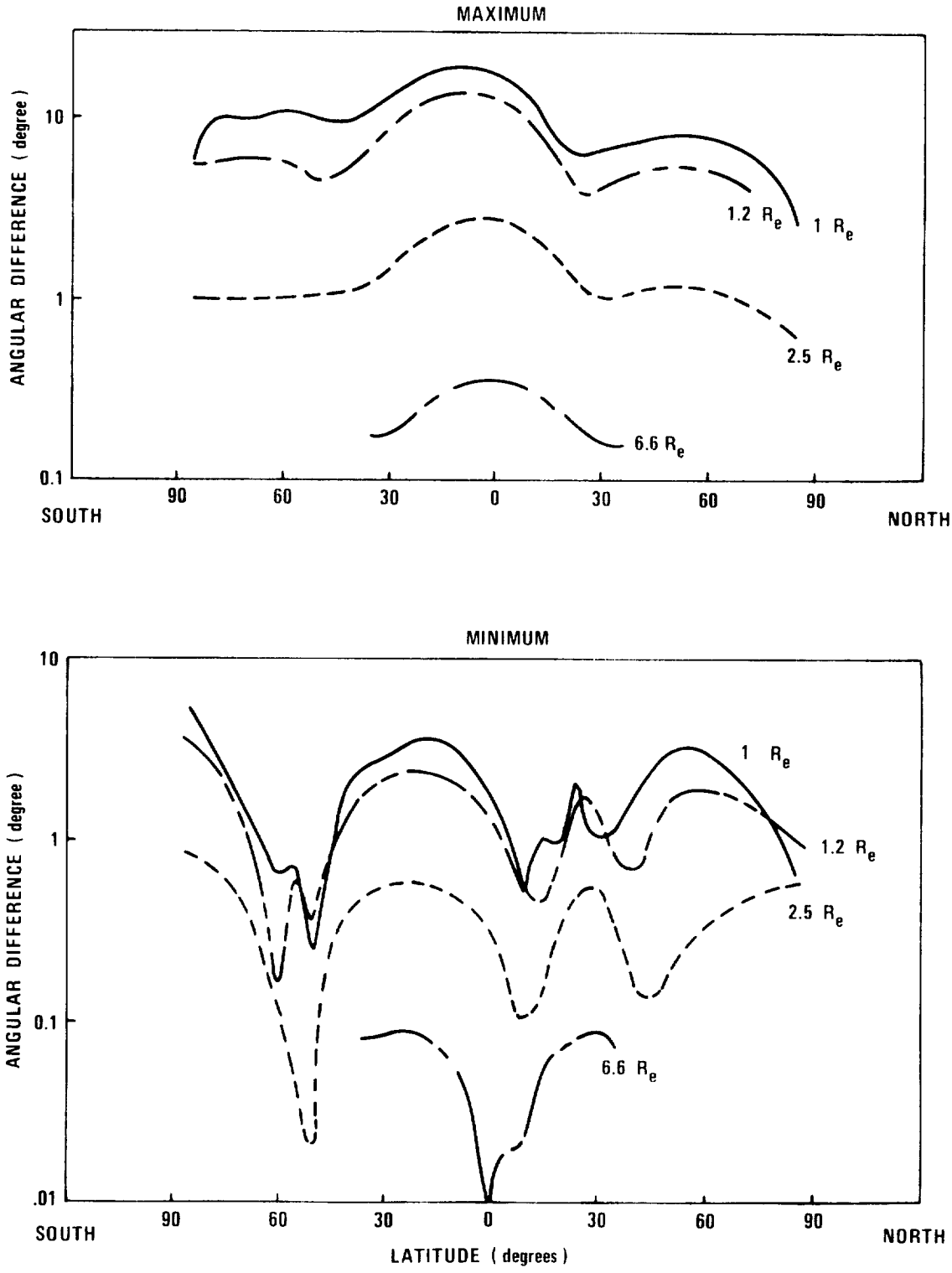

Figure C-6. –Maximum and minimum angular deviation of quadrupole model from spherical harmonic expansion model at selected geocentric distances (ref. 26).

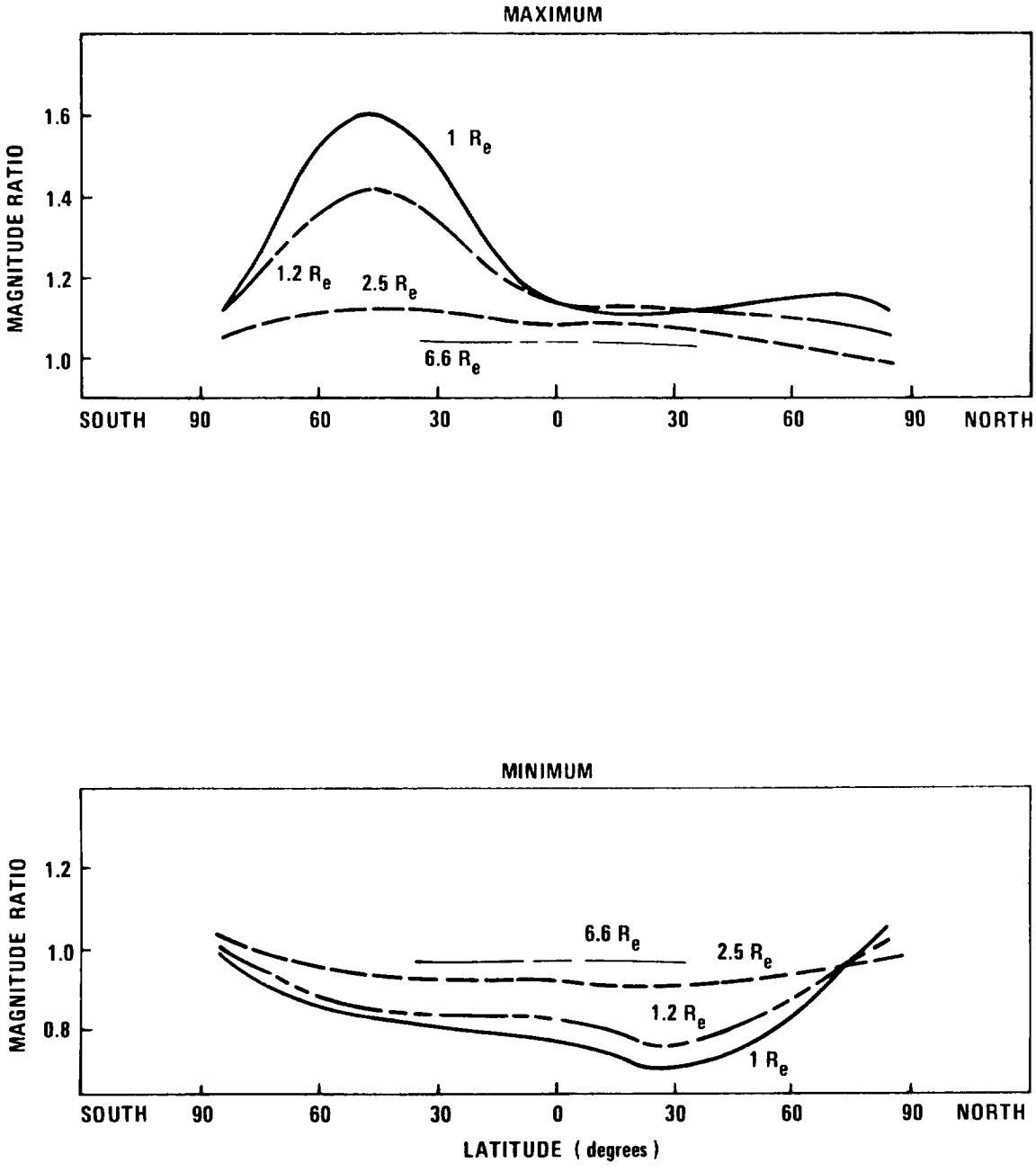

Figure C-7.–Maximum and minimum magnitude ratios of the tilted-dipole model to the spherical harmonic expansion model at selected geocentric distances (ref. 26).

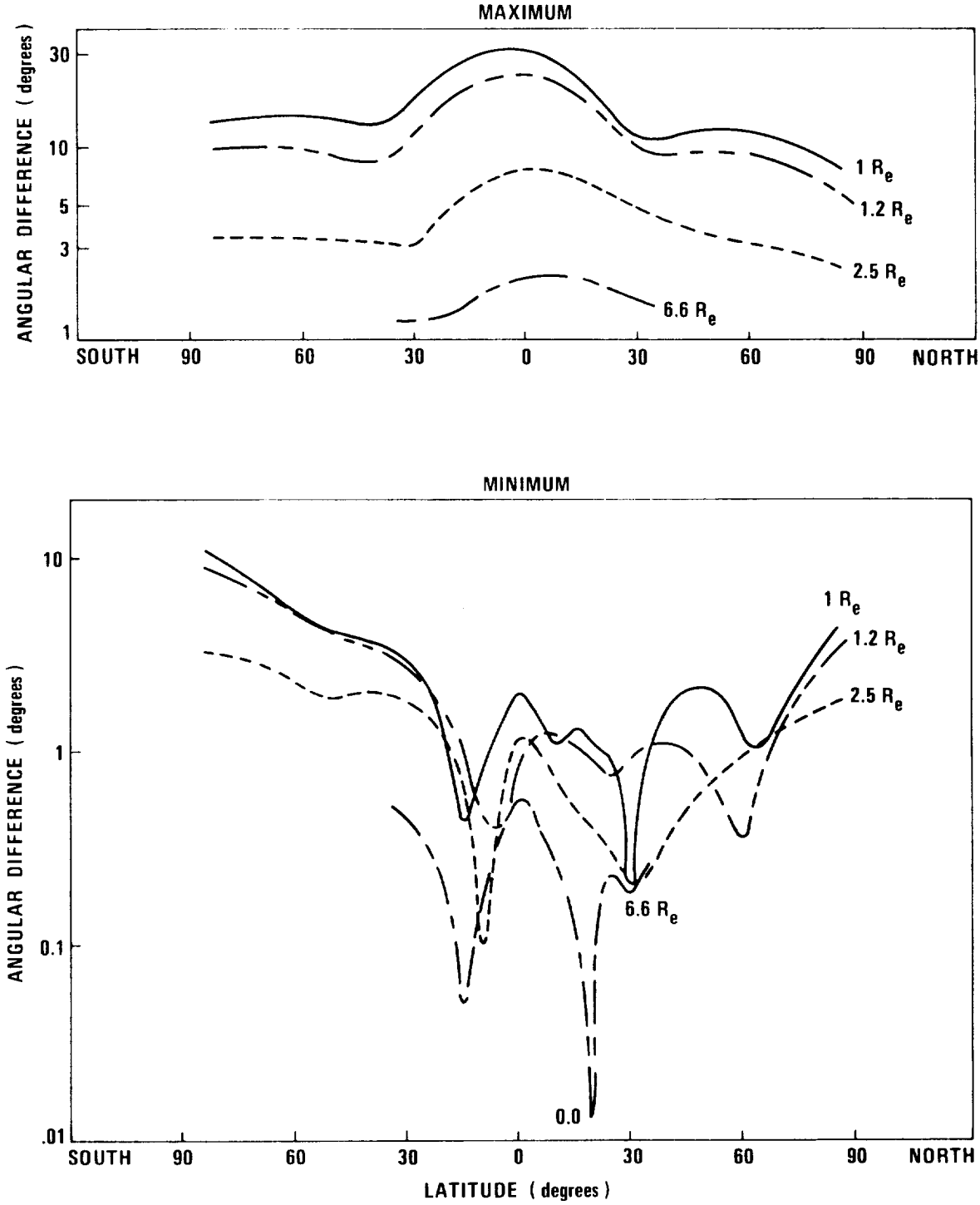

Figure C-8.–Maximum and minimum angular deviation of tilted-dipole model from spherical harmonic expansion model at selected geocentric distances (ref. 26).

NASA SPACE VEHICLE DESIGN CRITERIA MONOGRAPHS ISSUED TO DATE

SP-8001	(Structures)	Buffeting During Launch and Exit, May 1964
SP-8002	(Structures)	Flight-Loads Measurements During Launch and Exit, December 1964
SP-8003	(Structures)	Flutter, Buzz, and Divergence, July 1964
SP-8004	(Structures)	Panel Flutter, May 1965
SP-8005	(Environment)	Solar Electromagnetic Radiation, June 1965
SP-8006	(Structures)	Local Steady Aerodynamic Loads During Launch and Exit, May 1965
SP-8007	(Structures)	Buckling of Thin-Walled Circular Cylinders, September 1965 (Revised, August 1968)
SP-8008	(Structures)	Prelaunch Ground Wind Loads, November 1965
SP-8009	(Structures)	Propellent Slosh Loads, August 1968
SP-8010	(Environment)	Models of Mars Atmosphere (1967), May 1968
SP-8011	(Environment)	Models of Venus Atmosphere (1968), December 1968
SP-8012	(Structures)	Natural Vibration Model Analyses, September 1968
SP-8014	(Structures)	Entry Thermal Protection, August 1968
SP-8015	(Guidance and Control)	Guidance and Navigation for Entry Vehicles, November 1968
SP-8018	(Guidance and Control)	Spacecraft Magnetic Torques, March 1969
SP-8019	(Structures)	Buckling of Thin-Walled Truncated Cones, September 1968